Title: Resident Cardiac Macrophages Mediate Adaptive Myocardial Remodeling

Authors: Nicole R. Wong[1,*], Jay Mohan[1,*], Benjamin J Kopecky[1,*], Shuchi Guo[1,*], Lixia Du[2], Jamison Leid[1], Oleksandr Dmytrenko[1], Hannah Luehmann[3], Geetika Bajpai[1], Laura Ewald[1], Lauren Bell[1], Nikhil Patel[4], Inessa Lokshina[1], Andrea Bredemeyer[1], Carla J. Weinheimer[1], Jessica M. Nigro[1], Attila Kovacs[1], Sachio Morimoto[5], Peter O. Bayguinov[6], Max. R. Fisher[6], James A.J. Fitzpatrick[6,7], Slava Epelman[8], Daniel Kreisel[9,10], Rajan Sah[1], Yongjian Liu[3], Hongzhen Hu[2], Kory J. Lavine[1,9,11,#]

*authors contributed equally to this work

Affiliations:

[1]Center for Cardiovascular Research, Departmental of Medicine, Cardiovascular Division, Washington University School of Medicine, St. Louis, MO, USA

[2]Department of Anesthesiology, Washington University School of Medicine, St. Louis, MO, USA

[3]Department of Radiology, Washington University School of Medicine, St. Louis, MO, USA

[4]Center for Genome Sciences and Systems Biology, Departmental of Genetics, Washington University School of Medicine, St. Louis, MO, USA

[5]Department of Physical Therapy, International University of Health and Welfare, Fukuoka, Japan

[6]Washington University Center for Cellular Imaging, Washington University School of Medicine, St. Louis, MO, USA

[7]Departments of Neuroscience and Cell Biology & Physiology, and Biomedical Engineering, Washington University School of Medicine, St. Louis, MO, USA

[8]Toronto General Hospital Research Institute, University Health Network (UHN), Toronto ON, M5G 1L7, Canada

[9]Department of Pathology and Immunology, Washington University School of Medicine, St. Louis, MO, USA

[10]Department of Surgery, Washington University School of Medicine, St. Louis, MO, USA

[11]Department of Developmental Biology, Washington University School of Medicine, St. Louis, MO, USA

Key words: Macrophages ▪ C-C chemokine receptor 2 (CCR2) ▪ heart failure ▪ dilated cardiomyopathy ▪ cardiac remodeling ▪ angiogenesis ▪ transient receptor potential vanilloid 4 (TRPV4)

Running Title: Cardiac Macrophages and Chronic Heart Failure

[#]**Address for correspondence**
Kory J. Lavine MD, PhD
660 South Euclid Campus Box 8086
St. Louis, MO, 63110
Phone: 314 362-1171
Fax: 314 362-0186
Email: klavine@wustl.edu

Summary:

Cardiac macrophages represent a heterogeneous cell population with distinct origins, dynamics, and functions. Recent studies have revealed that C-C Chemokine Receptor 2 positive (CCR2+) macrophages derived from infiltrating monocytes regulate myocardial inflammation and heart failure pathogenesis. Comparatively little is known about the functions of tissue resident (CCR2-) macrophages. Herein, we identify an essential role for CCR2- macrophages in the chronically failing heart. Depletion of CCR2- macrophages in mice with dilated cardiomyopathy accelerated mortality and impaired ventricular remodeling and coronary angiogenesis, adaptive changes necessary to maintain cardiac output in the setting of reduced cardiac contractility. Mechanistically, CCR2- macrophages interacted with neighboring cardiomyocytes via focal adhesion complexes and were activated in response to mechanical stretch through a transient receptor potential vanilloid 4 (TRPV4) dependent pathway that controlled growth factor expression. These findings establish a role for tissue resident macrophages in adaptive cardiac remodeling and introduce a new mechanism of cardiac macrophage activation.

Introduction:

Paradigm shifting studies have demonstrated surprising heterogeneity among macrophage populations. It is now widely recognized that macrophages arise from distinct developmental origins including extraembryonic (yolk sac) and definitive hematopoietic progenitors and are maintained through differing mechanisms (Davies et al., 2013; Epelman et al., 2014b; Hashimoto et al., 2013; Hettinger et al., 2013; Hoeffel et al., 2015; Wynn et al., 2013; Yona et al., 2013). For example, microglia found within the brain are derived from extraembryonic hematopoiesis and maintained through local proliferation independent of monocyte input (Ginhoux et al., 2010), while macrophages that reside within the intestine are derived from definitive hematopoietic progenitors and are continually replenished by recruited monocytes (Bain et al., 2013). Most organs including the heart, lung, liver, and skin contain admixtures of distinct macrophage subsets with differing development origins, morphologies, tissue localizations, and population dynamics (Epelman et al., 2014a; Guilliams et al., 2013; Hoeffel et al., 2012; Theret et al., 2019). These findings have raised the possibility that individual macrophage subsets may execute unique and context specific functions.

Beyond regulating inflammatory signaling, macrophages contribute important functions to shaping and remodeling tissues throughout development and adulthood. Macrophages are essential for the development and maturation of the nervous and vascular systems, contribute to bone and tooth morphogenesis, and clear remnants of cells that undergo programmed cell death within the embryo (Fantin et al., 2010; Munoz-Espin et al., 2013; Parkhurst et al., 2013; Storer et al., 2013; Theret et al., 2019). Many of these macrophage populations originate from embryonic progenitors, reside within tissues for prolonged periods of time, and are referred to as tissue resident macrophages. Tissue resident macrophages also orchestrate regeneration of cardiac

and appendage tissue following amputation or other forms of injury (Aurora et al., 2014; Godwin et al., 2017; Godwin et al., 2013; Lavine et al., 2014; Petrie et al., 2014). In the adult organism, tissue resident macrophages play key roles in maintaining organ homeostasis and physiology including iron metabolism and transport, regulation of hematopoiesis, clearance of airway debris and surfactant, facilitation of electrical impulses through cardiac conduction tissue (Chow et al., 2011; Hashimoto et al., 2013; Hulsmans et al., 2017; Soares and Hamza, 2016). However, little is understood regarding the functions of tissue resident macrophages in the context of chronic disease.

Cardiac tissue remodeling is a widely recognized response to reductions in contractility, hemodynamic loading, or pathological insults to the heart. In these contexts, the heart undergoes robust geometric changes characterized by concentric thickening and dilation of the left ventricle (LV). While initially beneficial through reductions in LV wall stress, progressive myocardial hypertrophy and enlargement contributes to the development and progression of heart failure through cardiomyocyte cell death, further reduction in contractile function, and interstitial fibrosis. This process is referred to as adverse/pathological LV remodeling and is commonly observed across numerous cardiac pathologies such as myocardial infarction, viral myocarditis, and nonischemic cardiomyopathies (Burchfield et al., 2013; Xie et al., 2013).

It is important to note that not all forms of cardiac remodeling are maladaptive. Adaptive changes such as LV chamber enlargement and eccentric hypertrophy represent physiological adaptations to exercise conditioning. This physiological form of hypertrophy is associated with coronary angiogenesis, cardiomyocyte lengthening, and is distinct from adverse remodeling at the transcriptional level. Interstitial fibrosis and contractile dysfunction are typically not present in physiological hypertrophy (Nakamura

and Sadoshima, 2018). At present, the precise cellular and molecular mechanisms that orchestrate adaptive cardiac remodeling are incompletely understood. Intriguingly, features of adverse and adaptive LV remodeling coexist in patients with chronic heart failure highlighting the clinical relevance of understanding each form of cardiac tissue remodeling (Cohn et al., 2000; Patel et al., 2017).

Given their functions during heart development, cardiac tissue resident macrophages represent an attractive cell type that may govern remodeling of myocardial tissue in response to hemodynamic perturbations and/or chronic disease. Under homeostatic conditions, the adult heart contains a heterogeneous population of tissue resident macrophages that can be divided into two functionally distinct subsets based on the cell surface expression of C-C chemokine receptor 2 (CCR2) (Epelman et al., 2014a). CCR2+ macrophages are derived from definitive hematopoietic progenitors, replenished by monocyte recruitment and subsequent proliferation, and function to initiate inflammatory cascades. In response to cardiomyocyte death, CCR2+ macrophages produce inflammatory cytokines, orchestrate the recruitment of neutrophils and monocytes, generate damaging oxidative productions, and consequently, contribute to the progression of heart failure through collateral myocardial injury and adverse cardiac remodeling (Bajpai et al., 2019; Lavine et al., 2014; Li et al., 2016; Patel et al., 2018). Clinically, CCR2+ macrophage abundance is predictive of and associated with adverse LV remodeling in advanced heart failure patients (Bajpai et al., 2018), and thus, represent a target for future immunomodulatory therapies. CCR2- macrophages are largely derived from embryonic (yolk sac and fetal liver) hematopoietic progenitors and are maintained independent of monocyte recruitment through local proliferation. CCR2- macrophages orchestrate the maturation of the developing coronary vasculature and neonatal heart regeneration (Lavine et al., 2014; Leid et al., 2016). In the adult heart,

CCR2- macrophages appear to suppress inflammatory responses following acute myocardial injury (Bajpai et al., 2019). Whether CCR2- macrophages have similar reparative functions in the context of chronic heart failure is unknown.

Herein, we test the hypothesis that tissue resident CCR2- macrophages are involved in adaptive remodeling of the chronically failing heart. By employing a mouse model of dilated cardiomyopathy harboring a causative human mutation, we define the composition and dynamics of macrophages residing within the chronically failing heart. Through selective cell depletion studies, we reveal an essential role for CCR2- macrophages in adaptive LV remodeling, coronary angiogenesis, maintenance of cardiac output, and survival of mice with dilated cardiomyopathy. Furthermore, we provide evidence that mechanical sensing through a transient receptor potential vanilloid 4 (TRPV4) dependent pathway constitutes a novel mechanism controlling growth factor expression in tissue resident cardiac macrophages.

Results:

Cardiac Macrophage Heterogeneity in Dilated Cardiomyopathy. To investigate cardiac macrophage composition and function in chronic heart failure, we chose to focus on a mouse model of human dilated cardiomyopathy. Previously, knock-in mice were generated that harbor a causative mutation (ΔK210) in the endogenous Troponin T2 (Tnnt2) locus (Du et al., 2007). The Tnnt2$^{\Delta K210}$ mutation has been identified in numerous cohorts of familial and sporadic adult and pediatric dilated cardiomyopathy patients and is considered clinically as a pathogenic variant (McNally and Mestroni, 2017). Incorporation of the Tnnt2$^{\Delta K210}$ mutant protein into sarcomeres leads to reduced thin filament calcium sensitivity and cardiomyocyte contractility (Clippinger et al., 2019; Morimoto et al., 2002).

Consistent with previous reports, homozygous mice (Tnnt2$^{\Delta K210/\Delta K210}$) develop a dilated cardiomyopathy with profound LV remodeling (dilation and hypertrophy), reduced LV function (ejection fraction), and early mortality (**Fig. 1A-B and Fig. S1A**). Serial echocardiography revealed that Tnnt2$^{\Delta K210/\Delta K210}$ mice are born with reduced LV ejection fraction reflective of intrinsic impairment in cardiomyocyte contractility. LV remodeling (dilation and eccentric hypertrophy) was not evident until 2 weeks of age and increased progressively over time (**Fig. S1B**). These findings suggest that early LV remodeling may represent a compensatory response to reduced LV contractility.

To investigate the influence of chronic heart failure on cardiac macrophage abundance and composition, we examined histological sections obtained from control and Tnnt2$^{\Delta K210/\Delta K210}$ hearts. CD68 immunostaining revealed increased macrophage abundance at both 1 week and 8 weeks of age (**Fig. 1C, E and Fig. S1C-D**). Flow

cytometry demonstrated significant shifts in cardiac macrophage composition over time. At 1 week of age, Tnnt2$^{\Delta K210/\Delta K210}$ hearts displayed distributions of CCR2- macrophages, CCR2+ macrophages, and monocytes that were indistinguishable from controls. At 8 weeks of age, Tnnt2$^{\Delta K210/\Delta K210}$ hearts contained increased abundance of CCR2+ macrophages, CCR2- MHC-II^{low} macrophages, CCR2- MHC-II^{high} macrophages, and monocytes compared to controls. At 12 weeks of age, there was a progressive increase in the percentage of CCR2+ macrophages and marked increase in monocyte abundance (**Fig. 1D, F, Fig. S1E, Fig. S2**).

To non-invasively assess cardiac macrophage composition in intact mice, we took advantage of a positron emission tomography (PET) based molecular imaging strategy that detects CCR2+ macrophages (CCR2 PET) and total macrophages (CCR5 PET) previously established by our group (Heo et al., 2019; Luehmann et al., 2014). We observed robust CCR2 PET signal in the hearts of Tnnt2$^{\Delta K210/\Delta K210}$ mice compared to controls. Inclusion of Tnnt2$^{\Delta K210/\Delta K210}$ Ccr2$^{-/-}$ mice provided evidence of radiotracer specificity and ruled out the possibility that increased CCR2 PET signal was a result of expanded blood pool size. Consistent with greater numbers of total cardiac macrophages in Tnnt2$^{\Delta K210/\Delta K210}$ hearts, we observed increased CCR5 PET signal in the hearts of Tnnt2$^{\Delta K210/\Delta K210}$ mice compared to controls (**Fig. 1G-H**).

Analysis of RNA sequencing data comparing control and Tnnt2$^{\Delta K210/\Delta K210}$ hearts showed marked differences in gene expression that included pathways associated with collagen deposition, extracellular matrix organization, cell migration, and immune functions (**Fig. 1I**). Numerous differentially expressed genes have been implicated in macrophage activation and function (CD44, Mrc2, Nr4a1, Tlr4, Lbp, Csf2ra, Jun, Fos, Irf6, Socs2,

Chil1, Ctgf, Gdf15, Ifngr1, Maff) (**Fig. S3**), suggesting a potential role for macrophages in the chronically failing heart.

Origins and Dynamics of Cardiac Macrophages in Chronic Heart Failure. To delineate the contribution of monocytes to each cardiac macrophage population in the chronically failing heart, we bred Tnnt2$^{\Delta K210/\Delta K210}$ mice to CCR2^{gfp} knock-in mice to generate the following experimental groups: CCR2$^{gfp/+}$ (control), CCR2$^{gfp/gfp}$ (CCR2 KO), Tnnt2$^{\Delta K210/\Delta K210}$ CCR2$^{gfp/+}$ (heart failure), Tnnt2$^{\Delta K210/\Delta K210}$ CCR2$^{gfp/gfp}$ (heart failure, CCR2 KO). CCR2^{gfp} knock-in mice allow visualization of CCR2+ cells by immunostaining or flow cytometry in the absence of CCR2 protein expression or signaling (Satpathy et al., 2013). Immunostaining at 8 weeks of age demonstrated increased abundance of both CCR2- macrophages and CCR2+ macrophages in Tnnt2$^{\Delta K210/\Delta K210}$ hearts compared to controls. Deletion of CCR2 did not impact the abundance of CCR2- macrophages in non-failing or Tnnt2$^{\Delta K210/\Delta K210}$ hearts. Conversely, CCR2 deletion led to significant reductions in the abundance of CCR2+ macrophages in non-failing and Tnnt2$^{\Delta K210/\Delta K210}$ hearts (**Fig. S4A-B**). Flow cytometric analysis at 8 weeks of age confirmed selective reduction in CCR2+ macrophages in Tnnt2$^{\Delta K210/\Delta K210}$ CCR2$^{gfp/gfp}$ hearts compared to Tnnt2$^{\Delta K210/\Delta K210}$ CCR2$^{gfp/+}$ hearts (**Fig. S4C**). These data indicate that during this stage of chronic heart failure, CCR2- macrophages are maintained in the absence of monocyte input, whereas, CCR2+ macrophages require ongoing monocyte recruitment. Cell proliferation as assessed by Ki67 staining was exclusively increased in CCR2- macrophages in Tnnt2$^{\Delta K210/\Delta K210}$ hearts compared to controls (**Fig. S4D-E**).

To delineate the developmental origin of cardiac macrophages in the chronically failing heart, we crossed Tnnt2$^{\Delta K210/\Delta K210}$ mice to Flt3-Cre Rosa26-tdTomato mice. Flt3-Cre is

selectively active in definitive hematopoietic stem cells, and thus labels monocytes and macrophages derived from definitive hematopoiesis (Boyer et al., 2011). This strategy has extensively been used to distinguish macrophages derived from extraembryonic hematopoiesis from macrophages derived from definitive hematopoiesis (Epelman et al., 2014a; Lavine et al., 2014; Leid et al., 2016). Consistent with previous reports, >90% of CCR2+ macrophages in control hearts were tdTomato+ at both 1 and 12 weeks of age. Conversely, <40% of CCR2- macrophages in control hearts were tdTomato+ highlighting the significant contribution of extraembryonic hematopoiesis to this macrophage subset. The frequency of tdTomato+ positivity did not significantly differ between control and Tnnt2$^{\Delta K210/\Delta K210}$ hearts (**Fig. S4F-G**). Collectively, these findings indicate that in the context of chronic heart failure, CCR2- macrophages represent a mixed population of cells with contributions from extraembryonic and definitive hematopoiesis and are maintained by local proliferation in the absence of monocyte input. CCR2+ macrophages are exclusively derived from definitive hematopoiesis, long-lived, and maintained through gradual monocyte input.

Tissue Resident CCR2- and CCR2+ Macrophages Represent Functionally Distinct Populations in the Chronically Failing Heart. To gain insights into functional differences between macrophage populations that reside within the chronically failing heart, we performed gene expression profiling using a high sensitivity microarray platform. RNA was harvested from the following cell populations isolated from Tnnt2$^{\Delta K210/\Delta K210}$ Flt3-Cre Rosa26-tdTomato hearts using flow cytometry based cell sorting: CCR2+ macrophages (CCR2+MHC-II^{high}tdTomato+), CCR2-MHC-II^{low}tdTomato- macrophages, CCR2-MHC-II^{high}tdTomato- macrophages, CCR2-MHC-II^{low}tdTomato+ macrophages, CCR2-MHC-II^{high}tdTomato+ macrophages, and Ly6C^{high} monocytes

(Ly6C^{high}MHC-II^{low}CCR2+). Hierarchical clustering and principal component analysis revealed that the largest differences existed between CCR2- macrophages, CCR2+ macrophages, and Ly6C^{high} monocytes. CCR2+ macrophages clustered close to monocytes, which is consistent with ontological relationship between cell types. Importantly, each subset of CCR2- macrophages clustered together suggesting a high degree of similarity in gene expression amongst those populations (**Fig. 2A-B**).

Differential gene expression analysis demonstrated that 893 genes were differentially expressed between CCR2- macrophages and CCR2+ macrophages and 429 genes were differentially expressed between monocytes and macrophages using a threshold value of 1.5-fold and FDR adjusted p-value<0.05, highlighting the marked divergence between CCR2- macrophages and CCR2+ macrophages. Few differences were observed between individual CCR2- macrophage populations. Comparisons between CCR2- macrophages derived from definitive and extra-embryonic hematopoiesis revealed a single differentially expressed gene. Only 13 genes were differentially expressed between CCR2- MHC-II^{high} and CCR2- MHC-II^{low} populations, many of which were MHC-II alleles (**Fig. 2C**). Pathway analysis of genes differentially expressed between CCR2- macrophages and CCR2+ macrophages demonstrated that CCR2+ macrophages expressed genes associated with antigen presentation, immune/inflammatory response, T-cell co-stimulation, integrin signaling, and angiogenesis (**Fig. 2D-E**). Examples of genes upregulated in CCR2+ macrophages included Il1β, Gdf3, Lgals3, Ccl17, Cxcl19, Itgax, Itgb7, Itgax, Traf1, Tnip3, Tnfsf14, Timp1, Mmp12, Mmp19, Vegfa, Pgf, Col4a1, Col3a1, and Fn1. In contrast, CCR2- macrophages showed enrichment of pathways associated with endocytosis/transport, nervous system development, cell adhesion, and migration in CCR2- macrophages. CCR2- macrophages expressed a paucity of inflammatory mediators and instead

differentially expressed growth factors and genes associated with sensing mechanical stimuli including Igf1, Hbegf, Bmp2, Cyr61, Pdgfc, Fgf9, Trpv4, CD33, and Rhob (**Fig. 2F**).

CCR2- Macrophages are Required for Survival, Adaptive Tissue Remodeling, and Maintenance of Cardiac Output in the Chronically Failing Heart. We chose to focus on delineating the functions of CCR2- macrophages in the chronically failing heart, given their absolute abundance and unique gene expression signatures. We utilized CD169-DTR mice to selectively deplete CCR2- macrophages from the heart. We generated the following experimental groups: control, CD169-DTR, Tnnt2$^{\Delta K210/\Delta K210}$, and Tnnt2$^{\Delta K210/\Delta K210}$ CD169-DTR mice. Consistent with our previous findings (Bajpai et al., 2019), daily intraperitoneal administration of diphtheria toxin (DT) to CD169-DTR and Tnnt2$^{\Delta K210/\Delta K210}$ CD169-DTR mice led to marked reduction in cardiac macrophage density and selective elimination of CCR2- macrophages (**Fig. 3A-D**). Neutrophil, monocyte, and CCR2+ macrophage abundance was not impacted by CCR2- macrophages depletion. CCR2- macrophage depletion did not increase CCR2+ macrophage chemokine or cytokine expression or result in alteration in serum chemistries or cytokines (**Fig. S5-6**).

To assess whether CCR2- macrophages influence survival, cardiac function, and LV remodeling in the context of chronic heart failure, we treated control, CD169-DTR, Tnnt2$^{\Delta K210/\Delta K210}$, and Tnnt2$^{\Delta K210/\Delta K210}$ CD169-DTR mice with DT beginning at 6 weeks of age. The primary endpoints included a Kaplan-Meier survival analysis and echocardiographic assessment of LV function and remodeling performed at 9 weeks of age (3-weeks of DT treatment). Kaplan-Meier analysis revealed reduced survival of Tnnt2$^{\Delta K210/\Delta K210}$ CD169-DTR mice compared Tnnt2$^{\Delta K210/\Delta K210}$ mice. No mortality was

observed in control or CD169-DTR mice over the treatment period (**Fig. 3E**). Echocardiography demonstrated that similar reductions in LV ejection fraction between Tnnt2$^{\Delta K210/\Delta K210}$ mice and Tnnt2$^{\Delta K210/\Delta K210}$ CD169-DTR mice compared to controls **(Fig. 3F**). Tnnt2$^{\Delta K210/\Delta K210}$ mice displayed significantly greater LV remodeling (LV dilation and reduced relative LV wall thickness) compared to Tnnt2$^{\Delta K210/\Delta K210}$ CD169-DTR mice (**Fig. 3G-H**). Tnnt2$^{\Delta K210/\Delta K210}$ mice displayed increased LV stroke volumes compared to controls, whereas Tnnt2$^{\Delta K210/\Delta K210}$ CD169-DTR mice had lower LV stroke volumes compared to both control and Tnnt2$^{\Delta K210/\Delta K210}$ mice. (**Fig. 3I**). No differences were observed between control and CD169-DTR mice for all echocardiographic variables examined. Simultaneous measurement of LV pressure and volume confirmed reductions in LV end diastolic volume and stroke volume (measures of dilation) in Tnnt2$^{\Delta K210/\Delta K210}$ CD169-DTR compared to Tnnt2$^{\Delta K210/\Delta K210}$ mice (**Fig. 3J**). LV catheterization and dobutamine infusion revealed reduced LV end systolic pressure, myocardial contractility, and contractile reserve in Tnnt2$^{\Delta K210/\Delta K210}$ mice compared to controls. CCR2- macrophage depletion did not impact measurements of myocardial contractility in either wild type or Tnnt2$^{\Delta K210/\Delta K210}$ backgrounds (**Fig. 3K, Fig. S7**). Collectively, these findings indicate that CCR2- macrophage depletion blunts LV chamber remodeling in Tnnt2$^{\Delta K210/\Delta K210}$ mice without impacting myocardial contractility.

CCR2- Macrophages are Required for Myocardial Tissue Remodeling and Coronary Angiogenesis. We performed histological analysis following 3 weeks of DT treatment to examine whether structural differences within the myocardium explain reductions in LV dilation and remodeling in Tnnt2$^{\Delta K210/\Delta K210}$ CD169-DTR hearts. Compared to controls, Tnnt2$^{\Delta K210/\Delta K210}$ hearts displayed evidence of myocardial reorganization consisting of circumferential enlargement of the LV, loss of trabecular

myocardial tissue, and expansion of compact myocardial tissue. Tnnt2$^{\Delta K210/\Delta K210}$ CD169-DTR hearts displayed reduced circumferential LV enlargement, persistent trabecular myocardial tissue, and failed to expand the compact myocardium. CD169-DTR mice displayed no significant changes compared to controls (**Fig. 4A-C**). To verify these structural alterations by a second method, we performed X-Ray microscopy (XRM), a variant of micro-computed tomography (μCT). This technique provides full volume datasets enabling three-dimensional reconstruction of cardiac anatomy and virtual histology analysis. Surface projection and virtual histology images of the LV chamber revealed the presence of smooth appearing walls and precise alignment of muscle fibers in Tnnt2$^{\Delta K210/\Delta K210}$ hearts. In contrast, the LV walls of Tnnt2$^{\Delta K210/\Delta K210}$ CD169-DTR hearts displayed a more ribbon-like appearance and impaired muscle fiber alignment (**Fig. 4D**). Collectively, these findings indicate that CCR2- macrophages influence LV remodeling through alterations in myocardial tissue organization.

To examine whether CCR2- macrophages also affect cardiomyocyte size, we performed a morphometric analysis of cardiomyocytes isolated from control, Tnnt2$^{\Delta K210/\Delta K210}$, and Tnnt2$^{\Delta K210/\Delta K210}$ CD169-DTR hearts. Tnnt2$^{\Delta K210/\Delta K210}$ and Tnnt2$^{\Delta K210/\Delta K210}$ CD169-DTR cardiomyocytes demonstrated increased 2-dimensional area compared to cardiomyocytes isolated from control hearts. However, the extent of cell enlargement was greater in Tnnt2$^{\Delta K210/\Delta K210}$ cardiomyocytes compared to Tnnt2$^{\Delta K210/\Delta K210}$ CD169-DTR cardiomyocytes. Tnnt2$^{\Delta K210/\Delta K210}$ cardiomyocytes displayed increases in both cell width and length compared to control hearts. Interesting, Tnnt2$^{\Delta K210/\Delta K210}$ CD169-DTR cardiomyocytes displayed similar increases in cell width, but less extensive cell lengthening (**Fig. 4E-F**). These data suggest that modulation of cardiomyocyte length might also be involved in CCR2- macrophage dependent LV remodeling.

358

359 To evaluate whether CCR2- macrophages influence adverse/pathological LV
360 remodeling, we examined cardiomyocyte cross-sectional area, interstitial fibrosis, and
361 mRNA expression of established marker genes. Examination of cardiomyocyte cross-
362 sectional area *in situ* using wheat germ agglutinin stained sections demonstrated
363 increased cardiomyocyte area in both Tnnt2$^{\Delta K210/\Delta K210}$ and Tnnt2$^{\Delta K210/\Delta K210}$ CD169-DTR
364 hearts compared to controls. Of note, minimal evidence of interstitial fibrosis was evident
365 in this model at the stages examined (**Fig. S8A-D**). Nppa, Nppb, and Myh7 mRNA
366 expression was increased to a similar degree in Tnnt2$^{\Delta K210/\Delta K210}$ and Tnnt2$^{\Delta K210/\Delta K210}$
367 CD169-DTR hearts compared to controls (**Fig. S8E-G**). Previous studies have
368 implicated matrix metalloproteinase (MMP) activity in LV dilation and remodeling in the
369 context of myocardial infarction and injury models (Ducharme et al., 2000; Heymans et
370 al., 1999). We observed negligible MMP9 activity in the hearts of control and
371 Tnnt2$^{\Delta K210/\Delta K210}$ mice. Robust MMP9 activity was present in a mouse model of DT-
372 mediated cardiomyocyte ablation that mimics myocardial infarction (**Fig. S8H**).

373

374 Given previous findings that CCR2- macrophages regulate coronary angiogenesis in the
375 embryonic and neonatal heart (Lavine et al., 2014; Lavine et al., 2013; Leid et al., 2016),
376 we evaluated whether CCR2- macrophages also modulate coronary angiogenesis in the
377 context of chronic heart failure. Visualization of the coronary arterial vasculature using
378 Microfil casting demonstrated marked increases in epicardial coronary arterial
379 vasculature in Tnnt2$^{\Delta K210/\Delta K210}$ hearts compared to controls. Strikingly, we observed
380 expansion of the epicardial coronary arterial vasculature was markedly attenuated in
381 Tnnt2$^{\Delta K210/\Delta K210}$ CD169-DTR hearts (**Fig. 5A**). Measurement of coronary microvascular
382 density similarly revealed robust increases in Tnnt2$^{\Delta K210/\Delta K210}$ hearts compared to

controls and Tnnt2$^{\Delta K210/\Delta K210}$ CD169-DTR hearts (**Fig. 5B-C**). To explore potential mechanisms by which CCR2- macrophages promote coronary angiogenesis, we measured the expression pro-angiogenic growth factors expressed in CCR2- macrophages. Consistent with such a mechanism, Igf1, Pdgfc, Cyr61, and Hbegf mRNA expression was increased in CCR2- macrophages from Tnnt2$^{\Delta K210/\Delta K210}$ hearts compared to controls (**Fig. 5D**). Immunostaining analysis further revealed that macrophage IGF1 and CYR61 expression was increased in Tnnt2$^{\Delta K210/\Delta K210}$ hearts compared to controls. Increased macrophage IGF1 and CYR61 expression was not evident in Tnnt2$^{\Delta K210/\Delta K210}$ CD169-DTR hearts, presumably due to the absence of CCR2- macrophages (**Fig. 5E-F**). These observations indicate that CCR2- macrophages promote coronary angiogenesis in the context of chronic heart failure.

Previous work has suggested that cardiac macrophages have the potential to influence propagation of electrical signals through the atrioventricular node (Hulsmans et al., 2017). To assess whether alterations in electoral conduction occurred following depletion of CCR2- macrophages from control and Tnnt2$^{\Delta K210/\Delta K210}$ mice, we analyzed surface electrocardiograms (ECGs) obtained from anesthetized (isoflurane) control, CD169-DTR, Tnnt2$^{\Delta K210/\Delta K210}$, and Tnnt2$^{\Delta K210/\Delta K210}$ CD169-DTR mice treated with DT for 3 weeks. We did not observe significant differences in RR (heart rate), PR (atrioventricular node conduction), or QRS (intraventricular conduction) intervals between experimental groups. Tnnt2$^{\Delta K210/\Delta K210}$ and Tnnt2$^{\Delta K210/\Delta K210}$ CD169-DTR mice displayed prolongation of the QT (ventricular repolarization) interval compared to control and CD169-DTR mice. No significant differences were observed between Tnnt2$^{\Delta K210/\Delta K210}$ and Tnnt2$^{\Delta K210/\Delta K210}$ CD169-DTR mice for any examined parameter (**Fig. S9**). While these results indicate that defects in electrical propagation are unlikely to account for increased mortality

observed in Tnnt2$^{\Delta K210/\Delta K210}$ CD169-DTR mice, they do not rule out the possibility that CCR2- macrophages contribute to optimal cardiac conduction. Intriguingly, we found that both CCR2- and CCR2+ macrophages are located within the AV node potentially accounting for the lack of an overt electrical phenotype (**Fig. S10**).

A recent study suggested that tissue resident cardiac macrophages regulate myocardial metabolism and function through effects on mitochondrial homeostasis (Nicolas-Avila et al., 2020). To examine whether this might contribute to the phenotype of Tnnt2$^{\Delta K210/\Delta K210}$ CD169-DTR mice, we isolated mitochondria from control, CD169-DTR, Tnnt2$^{\Delta K210/\Delta K210}$, and Tnnt2$^{\Delta K210/\Delta K210}$ CD169-DTR hearts following 3 weeks of DT treatment. We did not detect any differences in mitochondrial respiration across experimental groups (**Fig. S11)**, indicating that alterations in mitochondrial function are unlikely responsible for the cardiac phenotype of Tnnt2$^{\Delta K210/\Delta K210}$ CD169-DTR mice.

CCR2- Macrophages Physically Interact with Neighboring Cardiomyocytes. To gain insights into how resident cardiac macrophages might influence myocardial remodeling and angiogenesis, we examined CCR2- and CCR2+ macrophage localization and structure in control and Tnnt2$^{\Delta K210/\Delta K210}$ hearts using three-dimensional confocal microscopy. Under baseline and heart failure conditions, CCR2- macrophages were observed within close proximity to cardiomyocytes and appeared to extend processes that contacted adjacent cardiomyocytes. CCR2+ macrophages were also found within the myocardium and extended processes within the interstitial space (**Fig. 6A-B**). Electron microscopy of Tnnt2$^{\Delta K210/\Delta K210}$ CCR2$^{gfp/+}$ hearts stained with anti-CD68 and anti-GFP antibodies confirmed that CCR2- macrophages were in close apposition to neighboring cardiomyocytes and revealed the presence of physical contacts between

these two cell types (**Fig. 6C**). CCR2+ macrophages were also found within the myocardium and extended processes into the interstitial space but did not directly contact cardiomyocytes (**Fig. 6D**). The projection length of CCR2- macrophages was greater in Tnnt2$^{\Delta K210/\Delta K210}$ hearts compared to controls. The projection length of CCR2+ macrophages was indistinguishable between control and Tnnt2$^{\Delta K210/\Delta K210}$ CCR2$^{gfp/+}$ hearts (**Fig. 6E**).

To characterize the temporal dynamics of how CCR2- macrophages interact with adjacent cardiomyocytes *in situ*, we performed two-photon microscopy on isolated mouse papillary muscle preparations. Papillary muscles were isolated from Cx$_3$cr1$^{GFP/+}$ Ccr2$^{RFP/+}$ mice and imaged for 1-2 hours in a temperature-controlled imaging chamber containing oxygenated media. Cellular processes were observed that extended from CCR2- macrophages and formed stable contacts with neighboring cardiomyocytes. These processes did not further extend or retract over the 90-minute time course of imaging (**Fig. 6F, supplemental movie**). Predominately CCR2- macrophages interacted with cardiomyocytes (**Fig. 6G**).

We did not observe electron densities indicative of desmosomes, adherens junctions, or tight junctions between CCR2- macrophages and cardiomyocytes. Immunostaining for α-cadherin (adherens conjunctions), desmoplakin (desmosomes), claudin (tight conjunctions), and Cx43 (gap junctions) revealed infrequent co-localization of these markers at sites of macrophage-cardiomyocyte interactions. Instead, we found that FAK and Paxillin (markers of focal adhesion complexes) were frequently present between CCR2- macrophages and cardiomyocytes (**Fig. 6H-I, Fig. S12**).

458 We then utilized an *in vitro* system to delineate whether focal adhesion complexes were
459 responsible for macrophage-cardiomyocyte interactions. We found that HL-1
460 cardiomyocytes and bone marrow-derived macrophages formed spontaneous
461 interactions when co-cultured. Electron microscopy revealed evidence of physical
462 interaction between HL1-cells and cardiomyocytes. Electron densities consistent with
463 desmosomes, adherens, tight, or gap junctions were not evident. Immunostaining
464 showed presence of Paxillin staining at sites of interactions between HL-1 cells and
465 bone marrow-derived macrophages (**Fig. S13**).
466
467 As previous studies have established that β-integrins are essential for formation of focal
468 adhesion complexes (Parsons et al., 2010), we focused our attention on inhibiting β-
469 integrin binding. Addition of RDG peptides or antibodies that blocked either β1-integrin or
470 β2-integrin binding was sufficient to disrupt interactions between HL-1 cells and bone
471 marrow-derived macrophages. Application of β1-integrin neutralizing antibodies also
472 resulted in loss of macrophage Paxillin staining at sites of cardiomyocyte-macrophage
473 interaction (**Fig. S14**). Collectively, these findings indicate that CCR2- macrophages
474 physically interact with cardiomyocytes and form focal adhesion complexes at sites of
475 cell-cell contacts.
476
477 **TRPV4 Regulates Growth Factor Expression in Macrophages.** Based on their
478 morphology and physical interaction with neighboring cardiomyocytes, we considered
479 the possibility that CCR2- macrophages may be activated by mechanical cues in the
480 context of heart failure. Specifically, we proposed that elevated LV chamber pressure
481 and resultant increased LV myocardial wall stress may be sensed by CCR2-
482 macrophages through their interactions with neighboring cardiomyocytes. To explore this

concept, we assayed the expression of known mechanoresponsive factors and found that TRPV4 mRNA was abundantly expressed in CCR2- macrophages (**Fig. 7A, Fig. S15**). Ratiometric calcium assays demonstrated that the TRPV4 channel was active in cardiac macrophages. Treatment of CCR2- and CCR2+ macrophages isolated from the heart by flow cytometry with a highly specific TRPV channel activator (GSK101) or TRPV4 channel inhibitor (GSK219) confirmed functional expression of TRPV4 protein in both CCR2- and CCR2+ macrophages within the ventricular myocardium (**Fig. 7B, Fig. S15**). Immunostaining of TRPV4-GFP BAC transgenic mice provided further evidence the TRPV4 was predominately expressed in macrophages located within the LV myocardium (**Fig. 7C**). Flow cytometry demonstrated expression of TRPV4 in cardiac macrophages and neutrophils (**Fig. 7D, Fig. S16**). We additionally detected TRPV4 activity in cardiac macrophages *in situ* using CX3CR1-ertCre Rosa26-GCaMP6s/tdtomato reporter mice (Madisen et al., 2015), which allows visualization of macrophage cytoplasmic calcium by restricting GCaMP6s expression to macrophages. 2-photon imaging of papillary muscles isolated from CX3CR1-ertCre Rosa26-GCaMP6/tdTomato hearts placed under axial tension revealed GCaMP signal in cardiac macrophages. Application of a TRPV4 inhibitor (GSK219) suppressed GCaMP signal, indicating that TRPV4 channel activity is responsible for the observed rise in macrophage cytoplasmic calcium (**Fig. 7E-F, Fig. S17**).

To examine the possibility that TRPV4 mediates the activation of macrophages by mechanical cues, we first utilized bone marrow-derived macrophages. Ratiometric calcium assays confirmed that bone marrow-derived macrophages express functional TRPV4 channels (**Fig. 7G**). Immunostaining of bone marrow-derived macrophages co-cultured with HL1 cardiomyocytes revealed expression of TRPV4 expression at sites of macrophage and cardiomyocyte interaction (**Fig. S18**). We then subjected bone marrow-

509 derived macrophages to cyclic mechanical stretch. Cells were cultured on silicone
510 membranes coated with collagen and fibronectin. Membranes were then stretched (10%
511 deformation, 1 Hz) for 24 hours in the presence of vehicle control or GSK219 (TRPV
512 inhibitor). Following 24 hours of cyclic uniaxial stretch, both vehicle and TRPV4 inhibitor
513 treated macrophages elongated and aligned along the axis of membrane deformation
514 (**Fig. 7H**). Quantitative RT-PCR assays revealed that bone marrow-derived
515 macrophages expressed increased levels of Igf1, Hbegf, and Cyr61 mRNA in response
516 to mechanical stretch. Application of the TRPV4 channel inhibitor blocked this response
517 (**Fig. 7I**).
518
519 To determine whether canonical pathways involved in macrophage activation affected
520 the ability of mechanical stretch to induce macrophage growth factor expression, we
521 subjected control, Myd88$^{-/-}$ and Trif$^{-/-}$ bone marrow derived-macrophages to uniaxial
522 cyclic stretch. Quantitative RT-PCR assays demonstrated that deletion of MYD88 or
523 TRIF had no impact on the expression of Igf1, Hbegf, or Cyr61 (Fig. 7**J**). Further,
524 activators of MYD88 and TRIF signaling (LPS, PolyIC) were unable to increase the
525 expression of Igf1, Hbegf, or Cyr61 and mechanical stretch did not induce the
526 expression of inflammatory cytokines (**Fig. S19**). Collectively, these observations
527 indicate that mechanical stretch promotes growth factor expression from macrophages
528 through a TRPV4 dependent mechanism that is independent of MYD88 and TRIF
529 signaling.
530
531 **TRPV4 regulates IGF1 expression in CCR2- macrophages and is required for**
532 **coronary angiogenesis.** To assess the functional relevance of TRPV4 *in vivo*, we
533 treated control and Tnnt2$^{\Delta K210/\Delta K210}$ mice with either vehicle control, TRPV4 inhibitor, or
534 TRPV4 agonist beginning at 6 weeks of age. Immunostaining for CD68 and IGF1 after 2

days of treatment revealed that TRPV4 activity modulates cardiac macrophage IGF1 expression. Compared to controls, cardiac macrophages in Tnnt2$^{\Delta K210/\Delta K210}$ hearts expressed IGF1 at higher frequency and increased mean levels. Treatment of Tnnt2$^{\Delta K210/\Delta K210}$ mice with the TRPV4 inhibitor was sufficient to reduce IGF1 expression (frequency and mean levels) in cardiac macrophages. Conversely, mice treated with the TRPV4 agonist displayed increased IGF1 expression in cardiac macrophages (**Fig. 8A-B, Fig. S20**). These data indicate that TRPV4 regulates cardiac macrophage IGF1 expression *in vivo*.

To determine whether suppression of TRPV4 activity impairs reparative responses that are dependent on CCR2- macrophages, we treated control and Tnnt2$^{\Delta K210/\Delta K210}$ mice with a TRPV4 inhibitor daily for 2 weeks beginning at 6 weeks of age. Histological evaluation demonstrated persistence of trabecular myocardium in Tnnt2$^{\Delta K210/\Delta K210}$ hearts treated with the TRPV4 inhibitor, a phenotype that is reminiscent of depleting CCR2- macrophages (**Fig. 8C-D**). While TRPV4 inhibition had no impact on ejection fraction, we observed attenuated LV dilation in Tnnt2$^{\Delta K210/\Delta K210}$ mice treated with the TRPV4 inhibitor (**Fig. 8E**). Examination of the coronary vasculature revealed that vehicle treated Tnnt2$^{\Delta K210/\Delta K210}$ mice displayed evidence of coronary angiogenesis at the microvascular and macrovascular levels compared to vehicle treated control mice. Importantly, Tnnt2$^{\Delta K210/\Delta K210}$ mice treated with the TRPV4 inhibitor displayed marked reductions in CD34+ blood vessel density within the LV myocardium and reduced large coronary artery complexity and branching compared to vehicle treated Tnnt2$^{\Delta K210/\Delta K210}$ hearts. In contrast, treatment with the TRPV4 inhibitor had no impact on coronary microvascular density in control mice (**Fig. 8F-I**). Together, these observations demonstrate that TRPV4 channel activity is necessary for adaptive LV remodeling and coronary

560 angiogenesis in the context of dilated cardiomyopathy and suggest a novel mechanism
561 by which tissue resident cardiac macrophages contribute to the survival of the failing
562 heart.
563
564 **Discussion:**
565 Inflammation has long been associated with heart failure development, progression, and
566 prognosis. Strong clinical associations and mechanistic studies in model organisms have
567 established that monocytes and macrophages contribute to adverse LV remodeling and
568 heart failure pathogenesis. Unfortunately, clinical studies exploring the use of
569 corticosteroids and tumor necrosis factor (TNF) antagonists in heart failure and
570 myocardial infarction failed to show clinical efficacy dampening enthusiasm for the
571 development of immunomodulatory therapies (Chung et al., 2003; Mann, 2015; Murphy
572 et al., 2020; Parrillo et al., 1989). In fact, each of these treatment strategies was
573 associated with potential harm. One explanation for these disappointing results is that
574 distinct components of the innate immune system differentially contribute to disease
575 pathogenesis, tissue homeostasis and repair. If this holds true, strategies that broadly
576 target the innate immune system may have competing effects of not only limiting
577 myocardial inflammation, but also, suppressing beneficial innate immune functions such
578 as cardiac tissue repair.
579
580 Indeed, previous studies have strongly supported the division of labor concept in regards
581 to cardiac macrophages, which are the most abundant innate immune cell population
582 within the mouse and human heart (Bajpai et al., 2018; Epelman et al., 2014a; Pinto et
583 al., 2016; Pinto et al., 2012). In this manuscript, we provide evidence that tissue resident
584 CCR2- cardiac macrophages represent a protective population that mediates adaptive
585 remodeling and survival of the chronically failing heart. By employing a mouse model of

586 dilated cardiomyopathy harboring a causative human mutation, we demonstrate that
587 CCR2- macrophages were essential to maintain adequate cardiac output in the setting
588 of reduced cardiac contractility by promoting LV enlargement and expansion of the
589 coronary system at the macrovascular and microvascular levels. Intriguingly, we
590 revealed a novel mechanism of cardiac macrophage activation. Through formation of
591 stable focal adhesion complexes with neighboring cardiomyocytes, CCR2- macrophages
592 may sense mechanical stretch in response to elevated loading conditions (*i.e*., LV end
593 diastolic pressure). The contribution of focal adhesion complexes to mechanosensing is
594 well established (Geiger et al., 2009). Consistent with this notion, inhibition of the
595 mechanosensitive channel, TRPV4, drastically reduced CCR2- macrophage pro-
596 angiogenic growth factor expression and prevented coronary angiogenesis and
597 myocardial tissue remodeling in our mouse model of dilated cardiomyopathy.
598 Collectively, these findings establish an unanticipated role for cardiac macrophages in
599 adaptive remodeling of the chronically failing heart and introduce a new mechanism of
600 cardiac macrophage activation through sensing of myocardial stretch.
601
602 These findings have several important implications for the cardiovascular field. First, it is
603 widely recognized that LV dilation is one of the strongest predictors of heart failure
604 outcomes including mortality (Merlo et al., 2011). Whether this represents an associative
605 or causative relationship is not immediately apparent and ultimately may depend on the
606 underlying pathology and clinical context. Our observations indicate that LV dilation may
607 be adaptive in some scenarios as it preserved cardiac output through augmentation of
608 stroke volume. Second, previous studies have demonstrated that CCR2- macrophages
609 remain abundant within the myocardium of patients with chronic heart failure (Bajpai et
610 al., 2018). However, their function within this context was unknown. Using a mouse
611 model of genetic dilated cardiomyopathy, we reveal an indispensable role for CCR2-

612 macrophages. Depletion of CCR2- macrophages blunted myocardial tissue
613 reorganization, cardiomyocyte lengthening, LV chamber enlargement, and coronary
614 angiogenesis. Markers of pathological hypertrophy including increased cardiomyocyte
615 cross-sectional area and fetal gene expression were not affected. These data further
616 substantiate the division of labor between CCR2- and CCR2+ cardiac macrophage
617 populations and highlight dichotomous contributions to disease pathogenesis and
618 protective adaptations, respectively (Bajpai et al., 2019; Dick et al., 2019; Epelman et al.,
619 2014a; Hulsmans et al., 2018; Lavine et al., 2014; Leid et al., 2016). Therapeutically,
620 these findings indicate the need to develop strategies that preserve or enhance the
621 function of CCR2- macrophages. Such an approach may enhance coronary
622 angiogenesis and favor adaptive forms of LV remodeling, thus providing additive benefit
623 to established medications for heart failure (ACE inhibitors, ARNIs, beta blockers,
624 aldosterone antagonists), which target a separate mechanism (adverse remodeling).
625
626 Exciting work has recently implicated cardiac macrophages in facilitating electrical
627 conduction, particularly through the atrioventricular node (Hulsmans et al., 2017). Using
628 surface electrocardiography, we did not observe arrhythmias or clear alterations in PR,
629 RR, or QT intervals following depletion of CCR2- macrophages. These data do not
630 exclude the possibility that CCR2- and/or CCR2+ macrophages participate in aspects of
631 cardiac pacemaker function, electrical propagation, or arrhythmia susceptibility in our
632 dilated cardiomyopathy model. Additional depletion models and dedicated
633 electrophysiology studies including appropriate provocative maneuvers will be required
634 to address these important questions.
635
636
637 This study also provides new insights into the properties and functions of tissue resident
638 macrophages. Specifically, we found that CCR2- macrophages within the LV

myocardium display a stereotyped morphology where they interact with neighboring cardiomyocytes through the formation of focal adhesion complexes. It is not yet clear whether macrophages interact with the cardiomyocyte basement membrane or directly with cardiomyocytes themselves. Regardless, these structures are stable over time and have the potential to serve as sensors of mechanical deformations such as increased wall tension that may occur in the context of elevated preload or afterload. Consistent with this concept, we found that mechanical stretch serves as a stimulus for pro-angiogenic growth factor expression, a process that was dependent on the mechanoresponsive TRPV4 channel. This observation suggests that a key function of CCR2- macrophages may be to sense hemodynamic alterations and promote adaptive tissue remodeling. Future work will clarify the breadth of hemodynamic stimuli that might activate CCR2- macrophages, identify the exact signaling pathways triggered by TRPV4 channel activity, and determine whether this mechanism might be active in regions of the heart other than the LV.

As TRPV4 has been implicated in alveolar and intestinal macrophages (Hamanaka et al., 2010; Luo et al., 2018; Pairet et al., 2018), sensing of mechanical tissue deformation may constitute a conserved role of tissue resident macrophages throughout the body. The ability to directly interact with parenchymal cells and sensing mechanical inputs may reflect an additional division of labor between tissue resident and infiltrating monocyte-derived macrophages. TRPV4 may also play an essential role in phagocytosis-induced inflammation a mechanism that is involved in clearance of cellular debris following tissue injury (Dutta et al., 2020; Goswami et al., 2019; Mannaa et al., 2018; Scheraga et al., 2016). Interestingly, we found that activation of TRPV4 by cyclic mechanical stretch was not dependent on MYD88 or TRIF signaling. A recent manuscript has suggested that

Piezo1 activation may trigger TRPV4 channel opening providing a more direct link to mechanical stimulation (Swain et al., 2020).

Our study is not without limitations. We primarily focused on a genetic mouse model of dilated cardiomyopathy. It remains to be shown whether CCR2- macrophages function in a similar manner in other non-ischemic and ischemic heart failure models. Based on available literature (Bajpai et al., 2019), we chose to employ CD169-DTR mice to deplete CCR2- macrophages. This line depletes other macrophage populations outside of the heart and we cannot rule out the possibility that extra-cardiac macrophage populations contribute to some of the observed phenotypes. Finally, while CCR2- macrophages represent the most abundant cell type that express active TRPV4 channels, we cannot exclude the possibility that TRPV4 may also influence the function of other cell types within the heart. TRPV4 was expressed in CCR2+ macrophages, neutrophils, and in a small population of cardiac endothelial cells. The impact of TRPV4 in these cell types remains to be elucidated.

In conclusion, our findings establish a role for tissue resident CCR2- macrophages in adaptive cardiac tissue remodeling and survival of the chronically failing heart. Furthermore, we provide initial evidence of a novel mechanism of cardiac macrophage activation, whereby CCR2- macrophages sense myocardial stretch through a TRPV4 dependent pathway.

Acknowledgments

This project was made possible by funding provided from the Children's Discovery Institute of Washington University and St. Louis Children's Hospital (CH-II-2015-462, CH-II-2017-628), Foundation of Barnes-Jewish Hospital (8038-88), and the NHLBI (R01 HL138466, R01 HL139714). K.J.L. is supported by Burroughs Welcome Fund (1014782). Histology was performed in the DDRCC advanced imaging and tissue analysis core supported by Grant #P30 DK52574. Imaging was performed in the Washington University Center for Cellular Imaging (WUCCI) which is funded, in part by the Children's Discovery Institute of Washington University and St. Louis Children's Hospital (CDI-CORE-2015-505 and CDI-CORE-2019-813) and the Foundation for Barnes-Jewish Hospital (3770). D.K. is supported by NIH P01AI116501 and R01 HL094601, Veterans Administration Merit Review grant 1I01BX002730 and The Foundation for Barnes-Jewish Hospital. We acknowledge the McDonnel Genome Institute for their assistance in designing and performing the micro array and RNA sequencing analysis. We recognize the mouse cardiovascular phenotyping core for performing echocardiography and invasive hemodynamics studies. B.J. Kopecky was supported by the Principles in Cardiovascular Research Training Grant (T32 HL007081) and the Washington University Physician Scientist Training Program. H.H. was supported by grants from the NIH, R01DK103901, R01AR077183, and R01AA027065, the Department of Anesthesiology at Washington University School of Medicine. Y.L. is supported by NIH R35HL145212 and R01HL131908. XRM data was generated on a Zeiss Xradia Versa 520 3D X-Ray microscope which was purchased with support from the Office of Research Infrastructure Programs (ORIP), a part of the NIH Office of the Director under grant OD021694.

Author Contributions

N.W., J.M., B.K., and S.G. performed the immunostaining, blood vessel casting, histology, RNA sequencing, and cell culture experiments. G.B, A.B., and O.D. performed the flow cytometry experiments. S.G. and B.K. performed the 2-photon imaging studies. H.L. and Y.L. performed the PET imaging studies and processed the data. L.E. and L.B. assisted in the cull culture experiments. I.K. and J.L. assisted in the macrophage depletion and performed the mitochondrial respiration studies. N.P. assisted in analysis of the ECG studies. S.M. provided Tnnt2$^{\Delta K210}$ mice. M.R.F, P.O.B. and J.A.J.F. performed the x-ray microscopy studies. L.D. and H.H. performed the ratiometric calcium imaging studies. C.M, A.K., J.M.N. performed the cardiac catheterization experiments. S.E., D.K., and R.S. assisted with experimental design and critical review of the manuscript. K.L. is responsible for all aspects of this manuscript including experimental design, data analysis, and manuscript production.

Competing Interest Statement

The authors have no financial or competing interests to disclose.

REFERENCES:

Aurora, A.B., Porrello, E.R., Tan, W., Mahmoud, A.I., Hill, J.A., Bassel-Duby, R., Sadek, H.A., and Olson, E.N. (2014). Macrophages are required for neonatal heart regeneration. J Clin Invest *124*, 1382-1392.

Bain, C.C., Scott, C.L., Uronen-Hansson, H., Gudjonsson, S., Jansson, O., Grip, O., Guilliams, M., Malissen, B., Agace, W.W., and Mowat, A.M. (2013). Resident and pro-inflammatory macrophages in the colon represent alternative context-dependent fates of the same Ly6Chi monocyte precursors. Mucosal Immunol *6*, 498-510.

Bajpai, G., Bredemeyer, A., Li, W., Zaitsev, K., Koenig, A.L., Lokshina, I., Mohan, J., Ivey, B., Hsiao, H.M., Weinheimer, C.*, et al.* (2019). Tissue Resident CCR2- and CCR2+ Cardiac Macrophages Differentially Orchestrate Monocyte Recruitment and Fate Specification Following Myocardial Injury. Circ Res *124*, 263-278.

Bajpai, G., Schneider, C., Wong, N., Bredemeyer, A., Hulsmans, M., Nahrendorf, M., Epelman, S., Kreisel, D., Liu, Y., Itoh, A.*, et al.* (2018). The human heart contains distinct macrophage subsets with divergent origins and functions. Nat Med.

Boyer, S.W., Schroeder, A.V., Smith-Berdan, S., and Forsberg, E.C. (2011). All hematopoietic cells develop from hematopoietic stem cells through Flk2/Flt3-positive progenitor cells. Cell Stem Cell *9*, 64-73.

Burchfield, J.S., Xie, M., and Hill, J.A. (2013). Pathological ventricular remodeling: mechanisms: part 1 of 2. Circulation *128*, 388-400.

Chow, A., Lucas, D., Hidalgo, A., Mendez-Ferrer, S., Hashimoto, D., Scheiermann, C., Battista, M., Leboeuf, M., Prophete, C., van Rooijen, N.*, et al.* (2011). Bone marrow CD169+ macrophages promote the retention of hematopoietic stem and progenitor cells in the mesenchymal stem cell niche. J Exp Med *208*, 261-271.

Chung, E.S., Packer, M., Lo, K.H., Fasanmade, A.A., Willerson, J.T., and Anti, T.N.F.T.A.C.H.F.I. (2003). Randomized, double-blind, placebo-controlled, pilot trial of infliximab, a chimeric monoclonal antibody to tumor necrosis factor-alpha, in patients with moderate-to-severe heart failure: results of the anti-TNF Therapy Against Congestive Heart Failure (ATTACH) trial. Circulation *107*, 3133-3140.

Clippinger, S.R., Cloonan, P.E., Greenberg, L., Ernst, M., Stump, W.T., and Greenberg, M.J. (2019). Disrupted mechanobiology links the molecular and cellular phenotypes in familial dilated cardiomyopathy. Proc Natl Acad Sci U S A *116*, 17831-17840.

Cohn, J.N., Ferrari, R., and Sharpe, N. (2000). Cardiac remodeling--concepts and clinical implications: a consensus paper from an international forum on cardiac remodeling. Behalf of an International Forum on Cardiac Remodeling. J Am Coll Cardiol *35*, 569-582.

Davies, L.C., Jenkins, S.J., Allen, J.E., and Taylor, P.R. (2013). Tissue-resident macrophages. Nat Immunol *14*, 986-995.

Dick, S.A., Macklin, J.A., Nejat, S., Momen, A., Clemente-Casares, X., Althagafi, M.G., Chen, J., Kantores, C., Hosseinzadeh, S., Aronoff, L.*, et al.* (2019). Self-renewing resident cardiac macrophages limit adverse remodeling following myocardial infarction. Nat Immunol *20*, 29-39.

Du, C.K., Morimoto, S., Nishii, K., Minakami, R., Ohta, M., Tadano, N., Lu, Q.W., Wang, Y.Y., Zhan, D.Y., Mochizuki, M.*, et al.* (2007). Knock-in mouse model of dilated cardiomyopathy caused by troponin mutation. Circ Res *101*, 185-194.

Ducharme, A., Frantz, S., Aikawa, M., Rabkin, E., Lindsey, M., Rohde, L.E., Schoen, F.J., Kelly, R.A., Werb, Z., Libby, P.*, et al.* (2000). Targeted deletion of matrix metalloproteinase-9 attenuates left ventricular enlargement and collagen accumulation after experimental myocardial infarction. J Clin Invest *106*, 55-62.

781 Dutta, B., Arya, R.K., Goswami, R., Alharbi, M.O., Sharma, S., and Rahaman,
782 S.O. (2020). Role of macrophage TRPV4 in inflammation. Lab Invest *100*, 178-185.
783 Epelman, S., Lavine, K.J., Beaudin, A.E., Sojka, D.K., Carrero, J.A., Calderon,
784 B., Brija, T., Gautier, E.L., Ivanov, S., Satpathy, A.T*., et al.* (2014a). Embryonic and
785 adult-derived resident cardiac macrophages are maintained through distinct
786 mechanisms at steady state and during inflammation. Immunity *40*, 91-104.
787 Epelman, S., Lavine, K.J., and Randolph, G.J. (2014b). Origin and functions of
788 tissue macrophages. Immunity *41*, 21-35.
789 Fantin, A., Vieira, J.M., Gestri, G., Denti, L., Schwarz, Q., Prykhozhij, S., Peri, F.,
790 Wilson, S.W., and Ruhrberg, C. (2010). Tissue macrophages act as cellular chaperones
791 for vascular anastomosis downstream of VEGF-mediated endothelial tip cell induction.
792 Blood *116*, 829-840.
793 Geiger, B., Spatz, J.P., and Bershadsky, A.D. (2009). Environmental sensing
794 through focal adhesions. Nat Rev Mol Cell Biol *10*, 21-33.
795 Ginhoux, F., Greter, M., Leboeuf, M., Nandi, S., See, P., Gokhan, S., Mehler,
796 M.F., Conway, S.J., Ng, L.G., Stanley, E.R*., et al.* (2010). Fate mapping analysis reveals
797 that adult microglia derive from primitive macrophages. Science *330*, 841-845.
798 Godwin, J.W., Debuque, R., Salimova, E., and Rosenthal, N.A. (2017). Heart
799 regeneration in the salamander relies on macrophage-mediated control of fibroblast
800 activation and the extracellular landscape. NPJ Regen Med *2*.
801 Godwin, J.W., Pinto, A.R., and Rosenthal, N.A. (2013). Macrophages are
802 required for adult salamander limb regeneration. Proc Natl Acad Sci U S A *110*, 9415-
803 9420.
804 Goswami, R., Arya, R.K., Biswas, D., Zhu, X., and Rahaman, S.O. (2019).
805 Transient Receptor Potential Vanilloid 4 Is Required for Foreign Body Response and
806 Giant Cell Formation. Am J Pathol *189*, 1505-1512.
807 Guilliams, M., De Kleer, I., Henri, S., Post, S., Vanhoutte, L., De Prijck, S.,
808 Deswarte, K., Malissen, B., Hammad, H., and Lambrecht, B.N. (2013). Alveolar
809 macrophages develop from fetal monocytes that differentiate into long-lived cells in the
810 first week of life via GM-CSF. J Exp Med *210*, 1977-1992.
811 Hamanaka, K., Jian, M.Y., Townsley, M.I., King, J.A., Liedtke, W., Weber, D.S.,
812 Eyal, F.G., Clapp, M.M., and Parker, J.C. (2010). TRPV4 channels augment
813 macrophage activation and ventilator-induced lung injury. Am J Physiol Lung Cell Mol
814 Physiol *299*, L353-362.
815 Hashimoto, D., Chow, A., Noizat, C., Teo, P., Beasley, M.B., Leboeuf, M.,
816 Becker, C.D., See, P., Price, J., Lucas, D*., et al.* (2013). Tissue-resident macrophages
817 self-maintain locally throughout adult life with minimal contribution from circulating
818 monocytes. Immunity *38*, 792-804.
819 Heo, G.S., Kopecky, B., Sultan, D., Ou, M., Feng, G., Bajpai, G., Zhang, X.,
820 Luehmann, H., Detering, L., Su, Y*., et al.* (2019). Molecular Imaging Visualizes
821 Recruitment of Inflammatory Monocytes and Macrophages to the Injured Heart. Circ
822 Res.
823 Hettinger, J., Richards, D.M., Hansson, J., Barra, M.M., Joschko, A.C.,
824 Krijgsveld, J., and Feuerer, M. (2013). Origin of monocytes and macrophages in a
825 committed progenitor. Nat Immunol *14*, 821-830.
826 Heymans, S., Luttun, A., Nuyens, D., Theilmeier, G., Creemers, E., Moons, L.,
827 Dyspersin, G.D., Cleutjens, J.P., Shipley, M., Angellilo, A*., et al.* (1999). Inhibition of
828 plasminogen activators or matrix metalloproteinases prevents cardiac rupture but
829 impairs therapeutic angiogenesis and causes cardiac failure. Nat Med *5*, 1135-1142.
830 Hoeffel, G., Chen, J., Lavin, Y., Low, D., Almeida, F.F., See, P., Beaudin, A.E.,
831 Lum, J., Low, I., Forsberg, E.C*., et al.* (2015). C-Myb(+) erythro-myeloid progenitor-

832 derived fetal monocytes give rise to adult tissue-resident macrophages. Immunity *42*,
833 665-678.
834 Hoeffel, G., Wang, Y., Greter, M., See, P., Teo, P., Malleret, B., Leboeuf, M.,
835 Low, D., Oller, G., Almeida, F.*, et al.* (2012). Adult Langerhans cells derive
836 predominantly from embryonic fetal liver monocytes with a minor contribution of yolk
837 sac-derived macrophages. J Exp Med *209*, 1167-1181.
838 Hulsmans, M., Clauss, S., Xiao, L., Aguirre, A.D., King, K.R., Hanley, A., Hucker,
839 W.J., Wulfers, E.M., Seemann, G., Courties, G.*, et al.* (2017). Macrophages Facilitate
840 Electrical Conduction in the Heart. Cell *169*, 510-522 e520.
841 Hulsmans, M., Sager, H.B., Roh, J.D., Valero-Munoz, M., Houstis, N.E.,
842 Iwamoto, Y., Sun, Y., Wilson, R.M., Wojtkiewicz, G., Tricot, B.*, et al.* (2018). Cardiac
843 macrophages promote diastolic dysfunction. J Exp Med *215*, 423-440.
844 Lavine, K.J., Epelman, S., Uchida, K., Weber, K.J., Nichols, C.G., Schilling, J.D.,
845 Ornitz, D.M., Randolph, G.J., and Mann, D.L. (2014). Distinct macrophage lineages
846 contribute to disparate patterns of cardiac recovery and remodeling in the neonatal and
847 adult heart. Proc Natl Acad Sci U S A *111*, 16029-16034.
848 Lavine, K.J., Kovacs, A., Weinheimer, C., and Mann, D.L. (2013). Repetitive
849 myocardial ischemia promotes coronary growth in the adult mammalian heart. J Am
850 Heart Assoc *2*, e000343.
851 Leid, J., Carrelha, J., Boukarabila, H., Epelman, S., Jacobsen, S.E., and Lavine,
852 K.J. (2016). Primitive Embryonic Macrophages are Required for Coronary Development
853 and Maturation. Circ Res *118*, 1498-1511.
854 Li, W., Hsiao, H.M., Higashikubo, R., Saunders, B.T., Bharat, A., Goldstein, D.R.,
855 Krupnick, A.S., Gelman, A.E., Lavine, K.J., and Kreisel, D. (2016). Heart-resident
856 CCR2(+) macrophages promote neutrophil extravasation through TLR9/MyD88/CXCL5
857 signaling. JCI Insight *1*.
858 Luehmann, H.P., Pressly, E.D., Detering, L., Wang, C., Pierce, R., Woodard,
859 P.K., Gropler, R.J., Hawker, C.J., and Liu, Y. (2014). PET/CT imaging of chemokine
860 receptor CCR5 in vascular injury model using targeted nanoparticle. J Nucl Med *55*, 629-
861 634.
862 Luo, J., Qian, A., Oetjen, L.K., Yu, W., Yang, P., Feng, J., Xie, Z., Liu, S., Yin, S.,
863 Dryn, D.*, et al.* (2018). TRPV4 Channel Signaling in Macrophages Promotes
864 Gastrointestinal Motility via Direct Effects on Smooth Muscle Cells. Immunity *49*, 107-
865 119 e104.
866 Madisen, L., Garner, A.R., Shimaoka, D., Chuong, A.S., Klapoetke, N.C., Li, L.,
867 van der Bourg, A., Niino, Y., Egolf, L., Monetti, C.*, et al.* (2015). Transgenic mice for
868 intersectional targeting of neural sensors and effectors with high specificity and
869 performance. Neuron *85*, 942-958.
870 Mann, D.L. (2015). Innate immunity and the failing heart: the cytokine hypothesis
871 revisited. Circ Res *116*, 1254-1268.
872 Mannaa, M., Marko, L., Balogh, A., Vigolo, E., N'Diaye, G., Kassmann, M.,
873 Michalick, L., Weichelt, U., Schmidt-Ott, K.M., Liedtke, W.B.*, et al.* (2018). Transient
874 Receptor Potential Vanilloid 4 Channel Deficiency Aggravates Tubular Damage after
875 Acute Renal Ischaemia Reperfusion. Sci Rep *8*, 4878.
876 McNally, E.M., and Mestroni, L. (2017). Dilated Cardiomyopathy: Genetic
877 Determinants and Mechanisms. Circ Res *121*, 731-748.
878 Merlo, M., Pyxaras, S.A., Pinamonti, B., Barbati, G., Di Lenarda, A., and Sinagra,
879 G. (2011). Prevalence and prognostic significance of left ventricular reverse remodeling
880 in dilated cardiomyopathy receiving tailored medical treatment. J Am Coll Cardiol *57*,
881 1468-1476.

Morimoto, S., Lu, Q.W., Harada, K., Takahashi-Yanaga, F., Minakami, R., Ohta, M., Sasaguri, T., and Ohtsuki, I. (2002). Ca(2+)-desensitizing effect of a deletion mutation Delta K210 in cardiac troponin T that causes familial dilated cardiomyopathy. Proc Natl Acad Sci U S A *99*, 913-918.

Munoz-Espin, D., Canamero, M., Maraver, A., Gomez-Lopez, G., Contreras, J., Murillo-Cuesta, S., Rodriguez-Baeza, A., Varela-Nieto, I., Ruberte, J., Collado, M.*, et al.* (2013). Programmed cell senescence during mammalian embryonic development. Cell *155*, 1104-1118.

Murphy, S.P., Kakkar, R., McCarthy, C.P., and Januzzi, J.L., Jr. (2020). Inflammation in Heart Failure: JACC State-of-the-Art Review. J Am Coll Cardiol *75*, 1324-1340.

Nakamura, M., and Sadoshima, J. (2018). Mechanisms of physiological and pathological cardiac hypertrophy. Nat Rev Cardiol *15*, 387-407.

Nicolas-Avila, J.A., Lechuga-Vieco, A.V., Esteban-Martinez, L., Sanchez-Diaz, M., Diaz-Garcia, E., Santiago, D.J., Rubio-Ponce, A., Li, J.L., Balachander, A., Quintana, J.A.*, et al.* (2020). A Network of Macrophages Supports Mitochondrial Homeostasis in the Heart. Cell *183*, 94-109 e123.

Pairet, N., Mang, S., Fois, G., Keck, M., Kuhnbach, M., Gindele, J., Frick, M., Dietl, P., and Lamb, D.J. (2018). TRPV4 inhibition attenuates stretch-induced inflammatory cellular responses and lung barrier dysfunction during mechanical ventilation. PLoS One *13*, e0196055.

Parkhurst, C.N., Yang, G., Ninan, I., Savas, J.N., Yates, J.R., 3rd, Lafaille, J.J., Hempstead, B.L., Littman, D.R., and Gan, W.B. (2013). Microglia promote learning-dependent synapse formation through brain-derived neurotrophic factor. Cell *155*, 1596-1609.

Parrillo, J.E., Cunnion, R.E., Epstein, S.E., Parker, M.M., Suffredini, A.F., Brenner, M., Schaer, G.L., Palmeri, S.T., Cannon, R.O., 3rd, Alling, D.*, et al.* (1989). A prospective, randomized, controlled trial of prednisone for dilated cardiomyopathy. N Engl J Med *321*, 1061-1068.

Parsons, J.T., Horwitz, A.R., and Schwartz, M.A. (2010). Cell adhesion: integrating cytoskeletal dynamics and cellular tension. Nat Rev Mol Cell Biol *11*, 633-643.

Patel, B., Bansal, S.S., Ismahil, M.A., Hamid, T., Rokosh, G., Mack, M., and Prabhu, S.D. (2018). CCR2(+) Monocyte-Derived Infiltrating Macrophages Are Required for Adverse Cardiac Remodeling During Pressure Overload. JACC Basic Transl Sci *3*, 230-244.

Patel, M.D., Mohan, J., Schneider, C., Bajpai, G., Purevjav, E., Canter, C.E., Towbin, J., Bredemeyer, A., and Lavine, K.J. (2017). Pediatric and adult dilated cardiomyopathy represent distinct pathological entities. JCI Insight *2*.

Petrie, T.A., Strand, N.S., Yang, C.T., Rabinowitz, J.S., and Moon, R.T. (2014). Macrophages modulate adult zebrafish tail fin regeneration. Development *141*, 2581-2591.

Pinto, A.R., Ilinykh, A., Ivey, M.J., Kuwabara, J.T., D'Antoni, M.L., Debuque, R., Chandran, A., Wang, L., Arora, K., Rosenthal, N.A.*, et al.* (2016). Revisiting Cardiac Cellular Composition. Circ Res *118*, 400-409.

Pinto, A.R., Paolicelli, R., Salimova, E., Gospocic, J., Slonimsky, E., Bilbao-Cortes, D., Godwin, J.W., and Rosenthal, N.A. (2012). An abundant tissue macrophage population in the adult murine heart with a distinct alternatively-activated macrophage profile. PLoS One *7*, e36814.

Satpathy, A.T., Briseno, C.G., Lee, J.S., Ng, D., Manieri, N.A., Kc, W., Wu, X., Thomas, S.R., Lee, W.L., Turkoz, M.*, et al.* (2013). Notch2-dependent classical dendritic

cells orchestrate intestinal immunity to attaching-and-effacing bacterial pathogens. Nat Immunol *14*, 937-948.

Scheraga, R.G., Abraham, S., Niese, K.A., Southern, B.D., Grove, L.M., Hite, R.D., McDonald, C., Hamilton, T.A., and Olman, M.A. (2016). TRPV4 Mechanosensitive Ion Channel Regulates Lipopolysaccharide-Stimulated Macrophage Phagocytosis. J Immunol *196*, 428-436.

Soares, M.P., and Hamza, I. (2016). Macrophages and Iron Metabolism. Immunity *44*, 492-504.

Storer, M., Mas, A., Robert-Moreno, A., Pecoraro, M., Ortells, M.C., Di Giacomo, V., Yosef, R., Pilpel, N., Krizhanovsky, V., Sharpe, J.*, et al.* (2013). Senescence is a developmental mechanism that contributes to embryonic growth and patterning. Cell *155*, 1119-1130.

Swain, S.M., Romac, J.M., Shahid, R.A., Pandol, S.J., Liedtke, W., Vigna, S.R., and Liddle, R.A. (2020). TRPV4 channel opening mediates pressure-induced pancreatitis initiated by Piezo1 activation. J Clin Invest *130*, 2527-2541.

Theret, M., Mounier, R., and Rossi, F. (2019). The origins and non-canonical functions of macrophages in development and regeneration. Development *146*.

Wynn, T.A., Chawla, A., and Pollard, J.W. (2013). Macrophage biology in development, homeostasis and disease. Nature *496*, 445-455.

Xie, M., Burchfield, J.S., and Hill, J.A. (2013). Pathological ventricular remodeling: therapies: part 2 of 2. Circulation *128*, 1021-1030.

Yona, S., Kim, K.W., Wolf, Y., Mildner, A., Varol, D., Breker, M., Strauss-Ayali, D., Viukov, S., Guilliams, M., Misharin, A.*, et al.* (2013). Fate mapping reveals origins and dynamics of monocytes and tissue macrophages under homeostasis. Immunity *38*, 79-91.

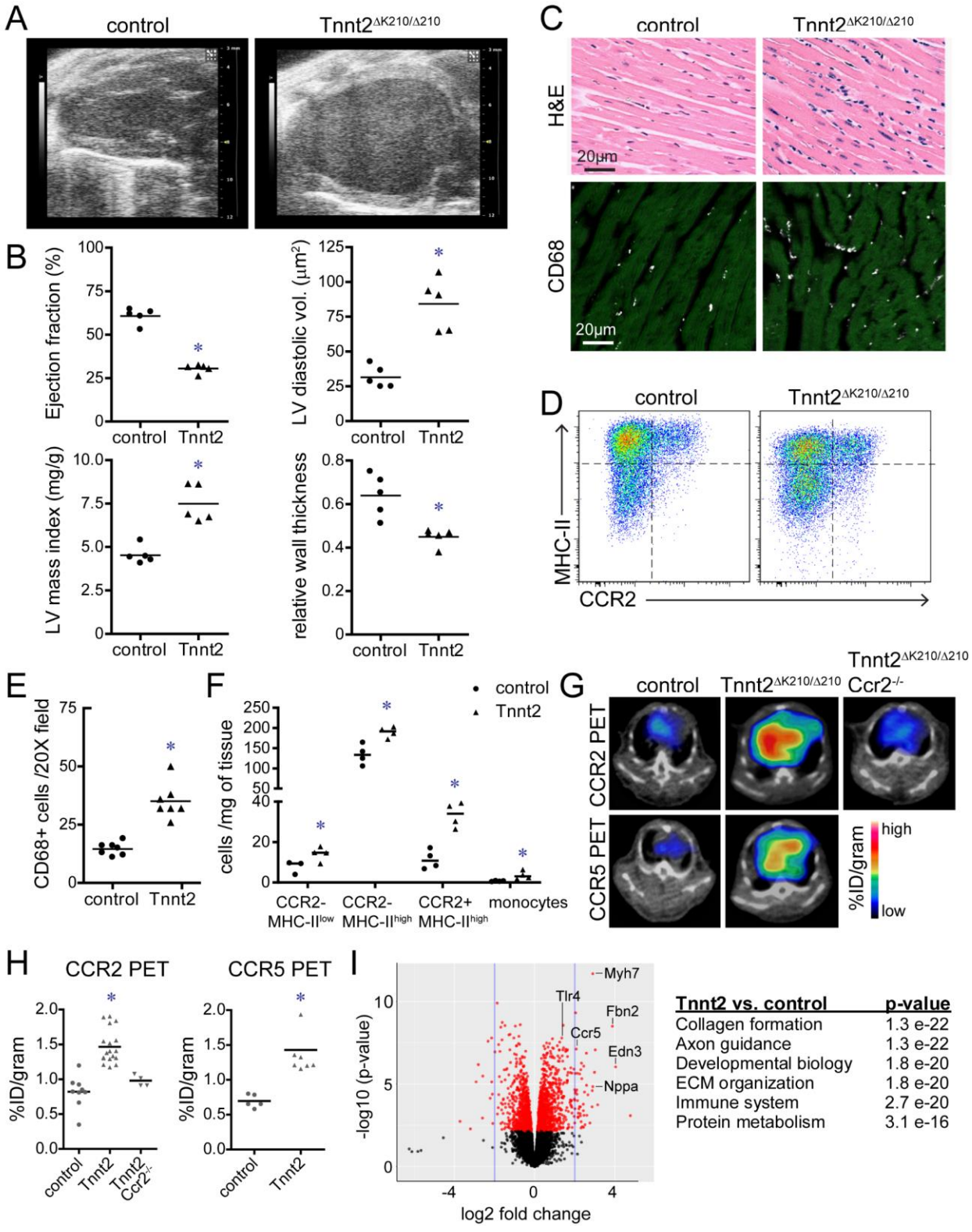

Tnnt2 vs. control	p-value
Collagen formation	1.3 e-22
Axon guidance	1.3 e-22
Developmental biology	1.8 e-20
ECM organization	1.8 e-20
Immune system	2.7 e-20
Protein metabolism	3.1 e-16

Figure 1. Expansion of cardiac macrophages in a mouse model of dilated cardiomyopathy. A, End-diastolic echocardiographic images of 8-week-old control and Tnnt2$^{\Delta K210/\Delta K210}$ mice. **B**, Quantification of ejection fraction, LV diastolic dimension, LV mass index, and relative wall thickness. **C**, H&E (top) and immunostaining images (bottom, CD68-white, cardiac actin-green) of 8-week-old control and Tnnt2$^{\Delta K210/\Delta K210}$ mice revealing expansion of cardiac macrophages in Tnnt2$^{\Delta K210/\Delta K210}$ mice compared to controls. Representative images from n=7 mice per experimental group. **D**, Representative flow cytometry plots of CD45^{+}Ly6G^{-} CD64^{+} macrophages showing increased abundance of CCR2- and CCR2+ macrophages in Tnnt2$^{\Delta K210/\Delta K210}$ mice compared to controls at 8 weeks of age. n=4 per experimental group. **E-F**, Quantification of CD68 immunostaining and flow cytometry. **G**, PET/CT images of control and Tnnt2$^{\Delta K210/\Delta K210}$ mice (6-10 weeks of age) using CCR2 and CCR5 tracers showing tracer uptake in the hearts of Tnnt2$^{\Delta K210/\Delta K210}$ mice. CCR2 signal is absent from Tnnt2$^{\Delta K210/\Delta K210}$ Ccr2$^{-/-}$ mice compared to controls. n=4-17 per experimental group. PET: positron emission tomography, CT: computed tomography. **H**, Quantification of CCR2 and CCR5 tracer uptake within the heart. **I**, MA plot and pathway analysis of RNA sequencing data comparing control to Tnnt2$^{\Delta K210/\Delta K210}$ hearts highlighting upregulated expression of transcripts associated with innate immunity in Tnnt2$^{\Delta K210/\Delta K210}$ hearts. n=5-6 per experimental group. For all panels, each data point denotes individual animals. * denotes $p<0.05$ (Mann-Whitney test) compared to controls.

A

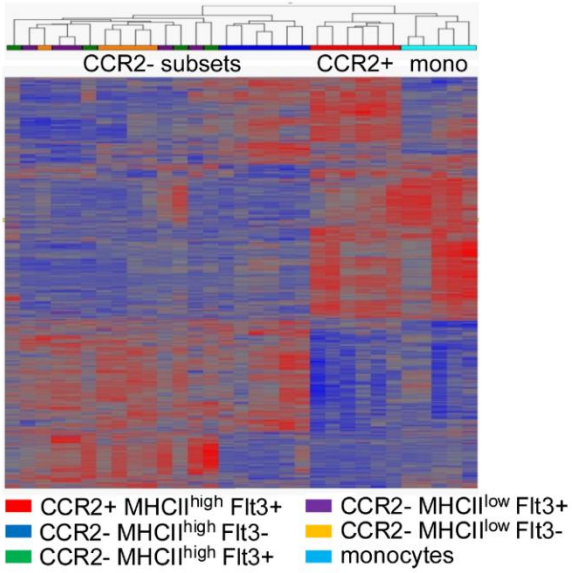

B

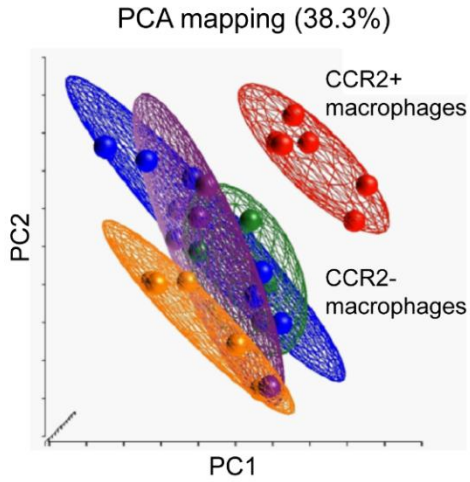

C

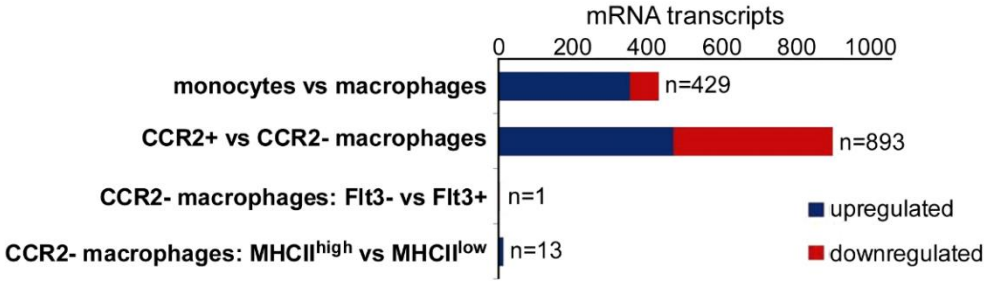

D

CCR2+ macrophages	p-value
Antigen processing/presentation	9.0 e-10
Immune response	4.6 e-9
Angiogensis	1.6 e-8
Inflammatory response	4.3 e-6
T-cell costimulation	6.8 e-4
Integrin signaling	8.4 e-4

E

CCR2- macrophages	p-value
Endocytosis	6.8 e-5
Transport	1.5 e-4
Nervous system development	2.2 e-3
Cell migration	2.6 e-3
Cell adhesion	2.8 e-3

F

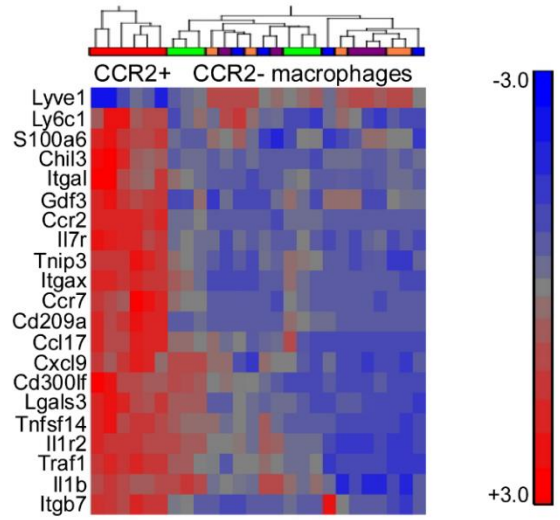

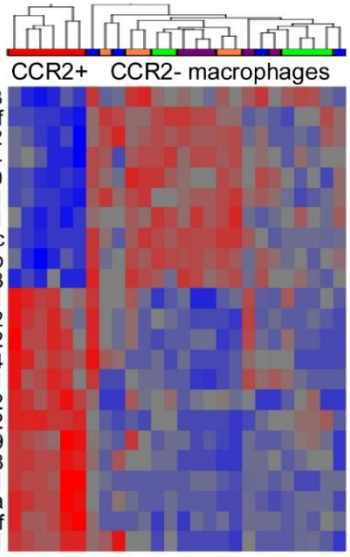

Figure 2. CCR2- and CCR2+ macrophages have distinct gene expression profiles in dilated cardiomyopathy. A, Hierarchical Clustering of CCR2+MHCII^{high} Flt3+, CCR2-MHCII^{low} Flt3-, CCR2-MHCII^{high} Flt3-, CCR2-MHCII^{low} Flt3+, CCR2-MHCII^{high} Flt3+, and CCR2+Ly6C^{high} monocytes FACS sorted from 8-week-old Tnnt2$^{\Delta K210/\Delta K210}$ mice. n=5-7 per experimental group. **B**, Principal component analysis (PCA) highlighting that CCR2+MHCII^{high} Flt3+ macrophages cluster independently from each of the CCR2- macrophage populations. Each data point represents biologically independent samples. **C**, Bar graph showing the number of differentially expressed genes (FDR $p<0.05$, fold change>1.5) for each of the listed comparisons. Blue: upregulated in Tnnt2$^{\Delta K210/\Delta K210}$ mice. Red: down regulated in Tnnt2$^{\Delta K210/\Delta K210}$ mice. **D**, Pathways enriched in CCR2+ and CCR2- (all subgroups combined) macrophages. **F**, Heat maps listing individual genes differentially expressed in CCR2+ and CCR2- macrophages. Scale bar denotes fold change.

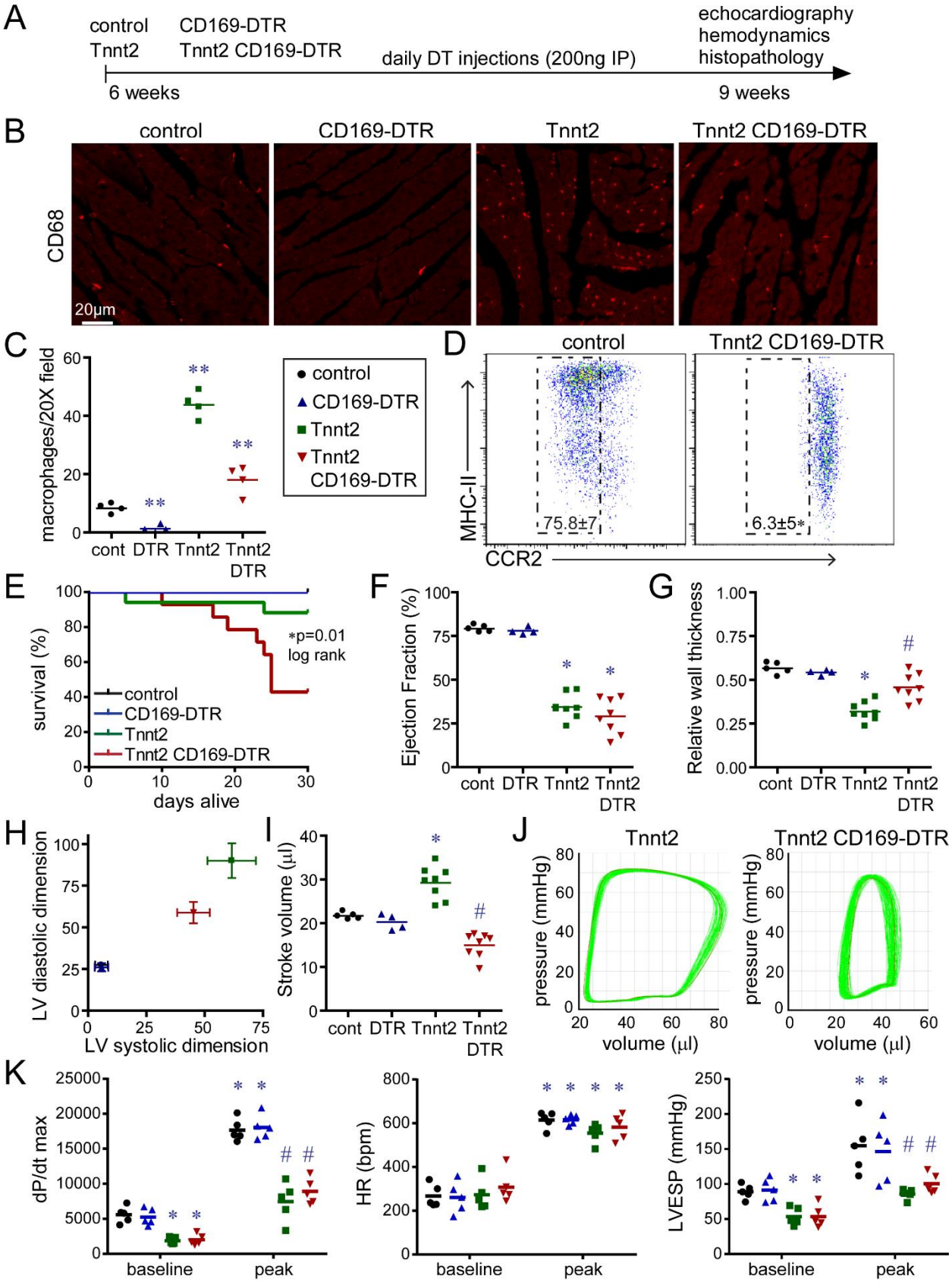

Figure 3. CCR2- macrophages influence survival and LV remodeling in dilated cardiomyopathy. A, Schematic outlining experimental groups, CCR2- macrophage depletion strategy, and analyzed endpoints. CCR2- macrophages were depleted by daily injection of diphtheria toxin (DT) into mice that expressed the diphtheria toxin receptor (DTR) under the control of the CD169 promoter. **B**, CD68 immunostaining of control, CD169-DTR, Tnnt2$^{\Delta K210/\Delta K210}$, and Tnnt2$^{\Delta K210/\Delta K210}$ CD169-DTR hearts after 3 weeks of DT treatment. N=4 per experimental group. **C**, Quantification of CD68 immunostaining. **D**, Flow cytometry plot of CD45^{+}Ly6G^{-}CD64^{+} macrophages showing specific depletion of CCR2- macrophages in Tnnt2$^{\Delta K210/\Delta K210}$ CD169-DTR hearts compared to controls. N=4 per experimental group. **E**, Kaplan-Meier analysis demonstrating reduced survival of Tnnt2$^{\Delta K210/\Delta K210}$ CD169-DTR compared to Tnnt2$^{\Delta K210/\Delta K210}$ mice. No mortality was evident in control and CD169-DTR mice over the analyzed time period. n=12-15 per experimental group. **F-I**, Echocardiographic assessment of LV ejection fraction, relative wall thickness, LV volumes (μl), and stroke volume in control, CD169-DTR, Tnnt2$^{\Delta K210/\Delta K210}$, and Tnnt2$^{\Delta K210/\Delta K210}$ CD169-DTR mice 3 weeks after DT treatment. n=4-8 per experimental group. **J**, Representative pressure volume loops showing reduced stroke volume in Tnnt2$^{\Delta K210/\Delta K210}$ CD169-DTR compared to Tnnt2$^{\Delta K210/\Delta K210}$ mice. n=4 per experimental group. **K**, Invasive hemodynamic measurements of LV dP/dt max, heart rate (HR), and LV end systolic pressure (LVESP) at baseline and during peak infusion of dobutamine (64 ng/min) in control, CD169-DTR, Tnnt2$^{\Delta K210/\Delta K210}$, and Tnnt2$^{\Delta K210/\Delta K210}$ CD169-DTR mice 3 weeks after DT treatment. n=5 per experimental group. Each data point denotes independent animals. Error bars denote standard deviation. * denotes $p<0.05$ (ANOVA, Post-hoc Tukey) compared to controls. # denotes $p<0.05$ compared to Tnnt2$^{\Delta K210/\Delta K210}$ mice.

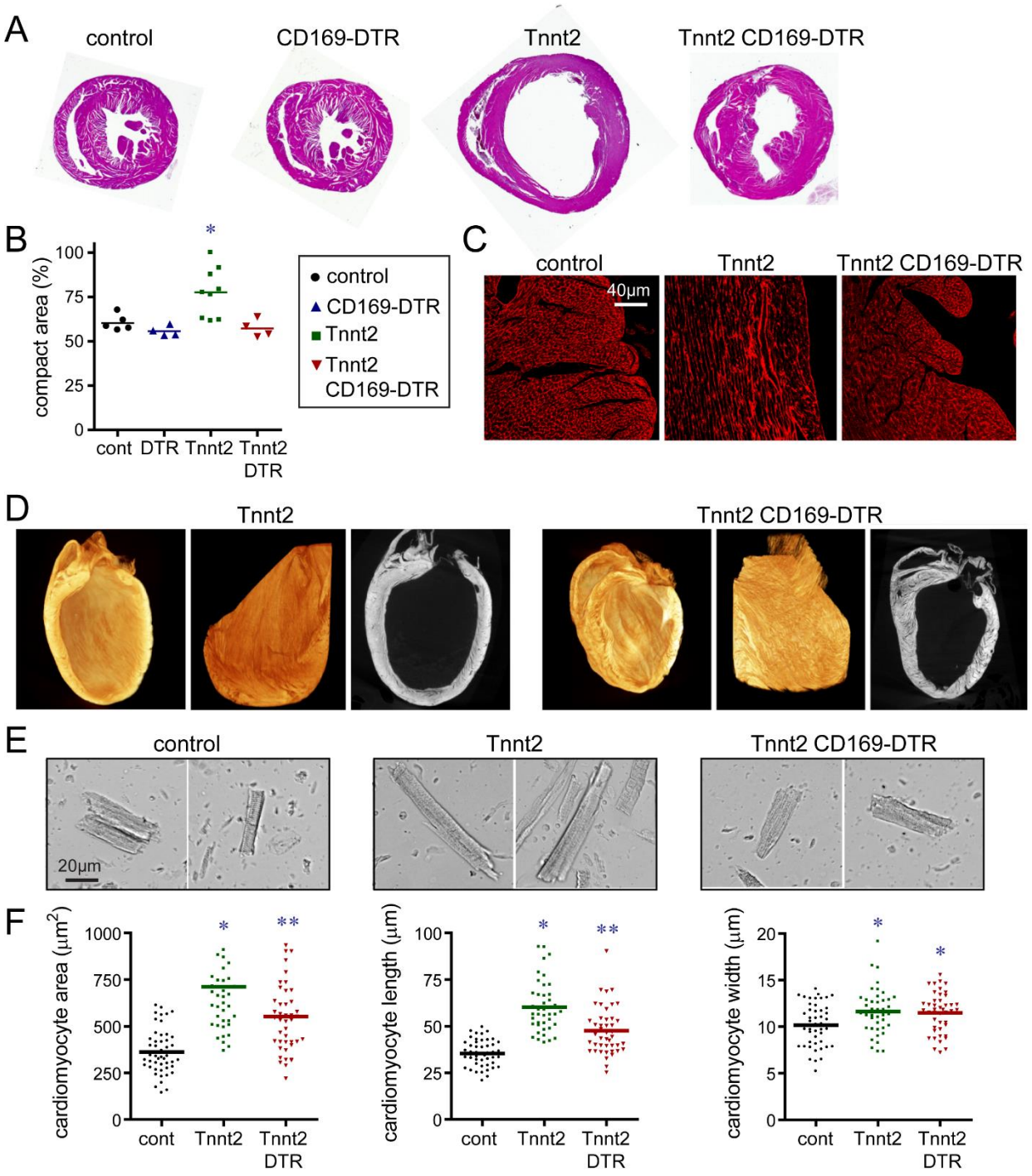

Figure 4. CCR2- macrophages orchestrate myocardial tissue adaptations in dilated cardiomyopathy. A, Low magnification H&E images of control, CD169-DTR, Tnnt2$^{\Delta K210/\Delta K210}$, and Tnnt2$^{\Delta K210/\Delta K210}$ CD169-DTR hearts (LV in cross-section) after 3 weeks of DT treatment. n=4-9 per experimental group. **B**, Quantification of the ratio of compact to trabecular myocardium in control, CD169-DTR, Tnnt2$^{\Delta K210/\Delta K210}$, and Tnnt2$^{\Delta K210/\Delta K210}$ CD169-DTR hearts. Each data point represents an individual animal. **C**, Wheat germ agglutinin (WGA, red) staining showing alterations in the alignment of trabecular cardiomyocytes in Tnnt2$^{\Delta K210/\Delta K210}$ compared to control hearts. The alignment of trabecular cardiomyocytes inTnnt2$^{\Delta K210/\Delta K210}$ CD169-DTR hearts is indistinguishable from controls. n=4-9 per experimental group. **D**, Reconstructed X-ray microscopy images and virtual histology comparing the myocardial architecture of Tnnt2$^{\Delta K210/\Delta K210}$ and Tnnt2$^{\Delta K210/\Delta K210}$ CD169-DTR hearts following 3 weeks of DT injection. n=4 per experimental group. The endocardial surface of Tnnt2$^{\Delta K210/\Delta K210}$ hearts is smooth and compacted whereas the endocardial surface of Tnnt2$^{\Delta K210/\Delta K210}$ CD169-DTR hearts has a rougher and meshwork-like appearance. **E**, Images of cardiomyocytes digested from control, Tnnt2$^{\Delta K210/\Delta K210}$, and Tnnt2$^{\Delta K210/\Delta K210}$ CD169-DTR hearts. Hearts were relaxed in potassium prior to fixation. **F**, Quantification of cardiomyocyte area, length, and width. Each data point represents individual cardiomyocytes analyzed from 4 independent animals per experimental group. * denotes $p<0.05$ (ANOVA, Post-hoc Tukey) compared to controls. ** denotes $p<0.05$ compared to control and Tnnt2$^{\Delta K210/\Delta K210}$ mice.

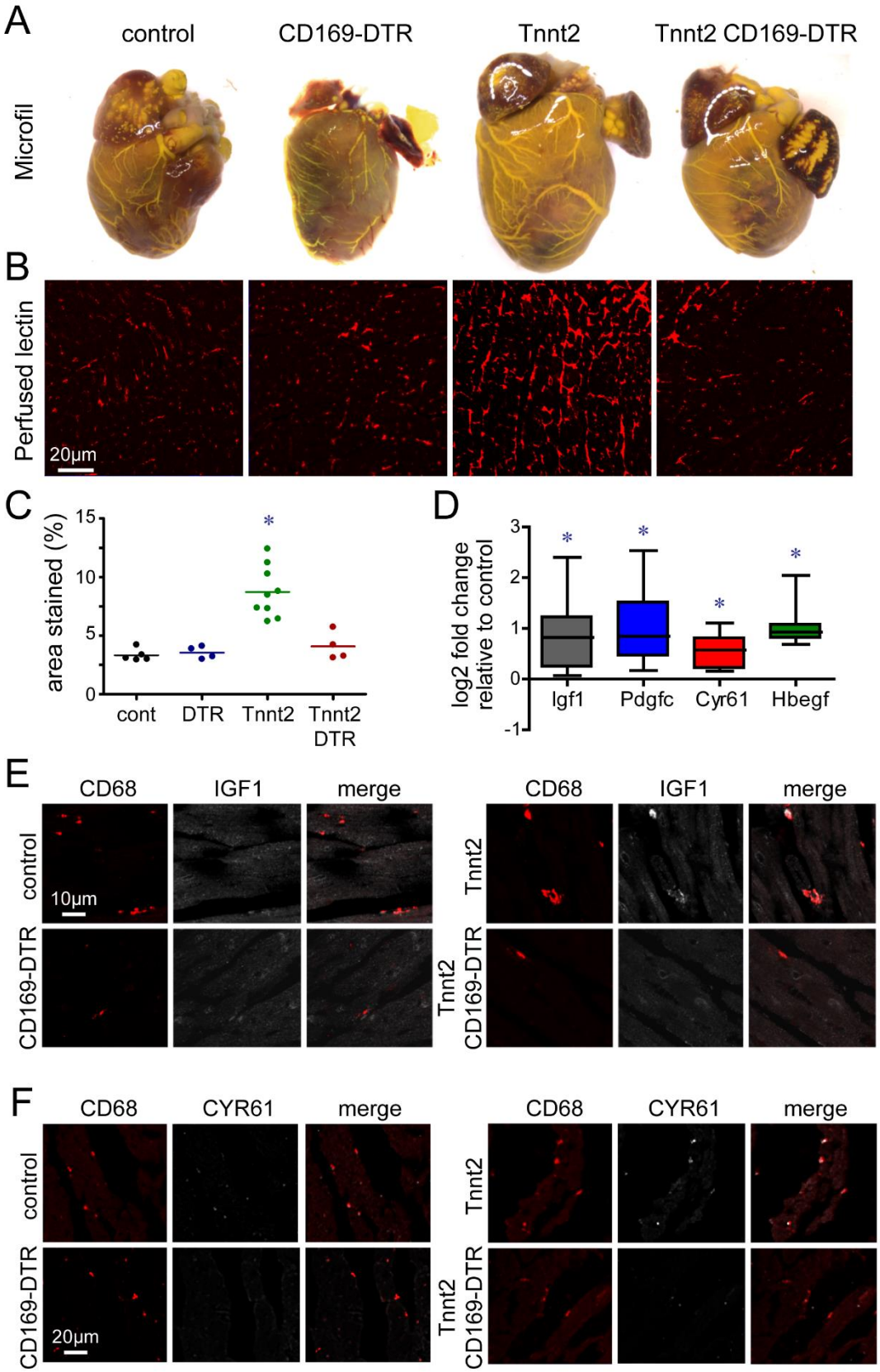

Figure 5. CCR2- macrophages are essential for coronary angiogenesis in dilated cardiomyopathy. A, Microfil vascular casting of control, CD169-DTR, Tnnt2$^{\Delta K210/\Delta K210}$, and Tnnt2$^{\Delta K210/\Delta K210}$ CD169-DTR hearts after 3 weeks of DT treatment. Tnnt2$^{\Delta K210/\Delta K210}$ hearts display marked expansion in the coronary macrovasculature that is diminished in Tnnt2$^{\Delta K210/\Delta K210}$ CD169-DTR hearts. n=4 per experimental group. **B**, Microvascular imaging (perfused lectin) of control, CD169-DTR, Tnnt2$^{\Delta K210/\Delta K210}$, and Tnnt2$^{\Delta K210/\Delta K210}$ CD169-DTR hearts after 3 weeks of DT treatment. Tnnt2$^{\Delta K210/\Delta K210}$ hearts display marked expansion in the coronary microvasculature that is diminished in Tnnt2$^{\Delta K210/\Delta K210}$ CD169-DTR hearts. n=4-9 per experimental group. **C**, Quantification of the coronary microvascular in control, CD169-DTR, Tnnt2$^{\Delta K210/\Delta K210}$, and Tnnt2$^{\Delta K210/\Delta K210}$ CD169-DTR hearts. Each data point represents an individual animal. * denotes $p<0.05$ (ANOVA, Post-hoc Tukey) compared to controls. **D**, CCR2- macrophages from Tnnt2$^{\Delta K210/\Delta K210}$ hearts display increased Igf1, Pdgfc, Cyr61, and Hbegf mRNA expression compared to CCR2- macrophages isolated from control mice. n=5 per experimental group. * denotes $p<0.05$ (Mann-Whitney test) compared to controls. **E-F**, Immunostaining of control, CD169-DTR, Tnnt2$^{\Delta K210/\Delta K210}$, and Tnnt2$^{\Delta K210/\Delta K210}$ CD169-DTR hearts after 3 weeks of DT treatment showing that macrophages within the LV myocardium of Tnnt2$^{\Delta K210/\Delta K210}$ mice display increased expression of IGF1 (E, white) and CYR61 (F, white). Red: CD68. n=5 per experimental group.

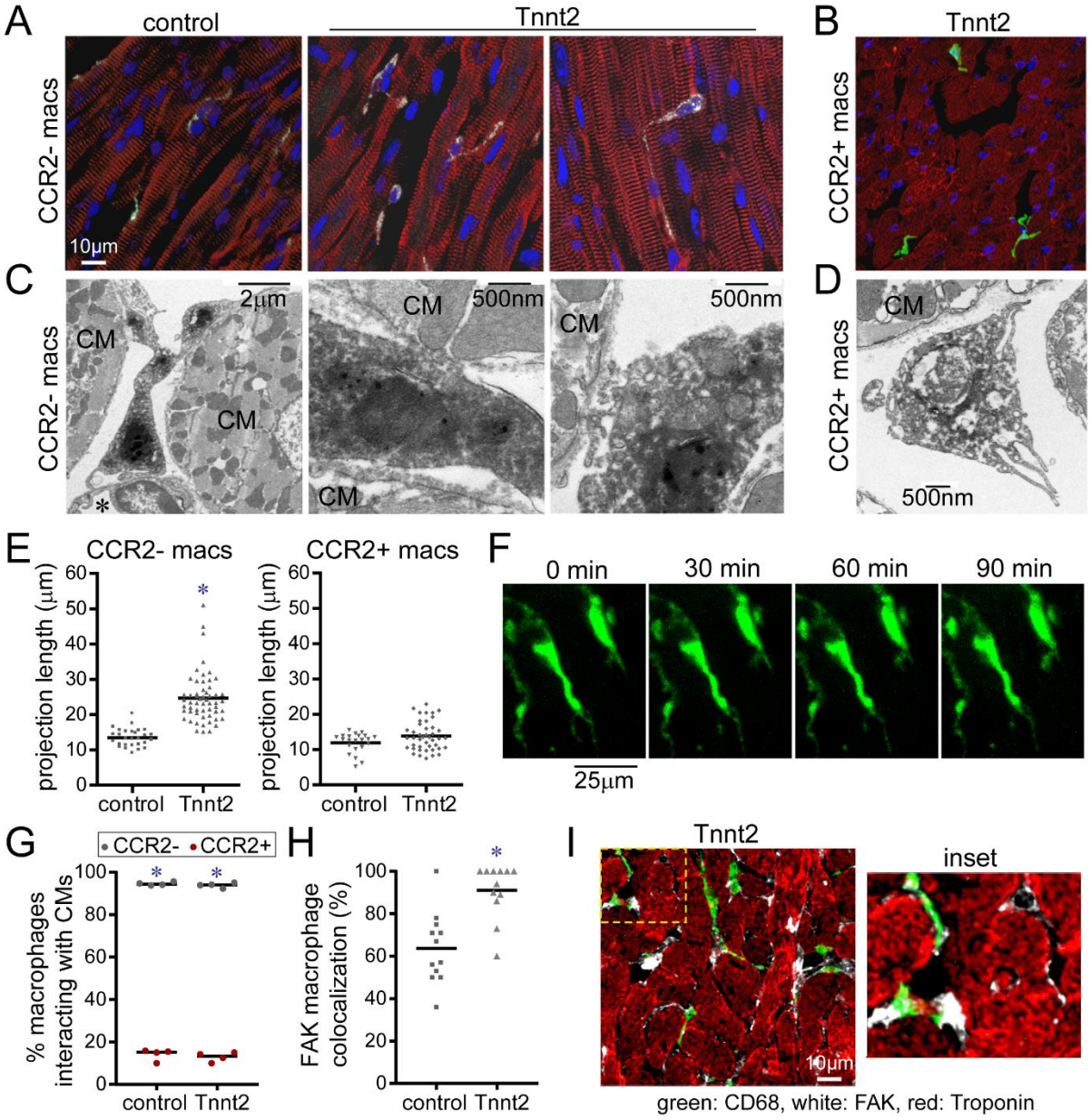

Figure 6. CCR2- macrophages interact with neighboring cardiomyocytes through focal adhesion complexes. A-B, Compressed Z-stack images showing distinct morphologies of CCR2- (A) and CCR2+ (B) cardiac macrophages in the LV myocardium of a 8-week-old control $CCR2^{GFP/+}$ and $Tnnt2^{\Delta K210/\Delta K210}$ $CCR2^{GFP/+}$ hearts. CCR2- cardiac macrophage projections are closely associated with neighboring cardiomyocytes whereas CCR2+ macrophage projections are shorter and remain localized to the interstitial space. n=4-6 per experimental group. CD68: white, GFP: green, α-actinin, red, DAPI: blue. **C-D**, Electron microscopy of CCR2- (C) and CCR2+ (D) cardiac macrophages in $Tnnt2^{\Delta K210/\Delta K210}$ $CCR2^{GFP/+}$ hearts. CCR2- macrophage are found adjacent to endothelial cells (*) and make contact with cardiomyocytes (CM). CCR2+ macrophages remain within the interstitial space between cardiomyocytes. n=4 per experimental group. **E**, Measurement of projection length in CCR2- and CCR2+ macrophages found within the myocardium of 8-week-old control $CCR2^{GFP/+}$ and $Tnnt2^{\Delta K210/\Delta K210}$ $CCR2^{GFP/+}$ hearts. * denotes $p<0.05$ (Mann-Whitney test) compared to controls. **F**, 2-photon microscopy of live $CX3CR1^{GFP/+}$ $CCR2^{RFP/+}$ papillary muscle cell preparations (n=4) showing that projections emanating from CCR2- macrophages (green) remain stable over 90 minutes. **G**, Quantification of the percent of CCR2- (black data points) and CCR2+ (red data points) macrophages interacting with cardiomyocytes in control and $Tnnt2^{\Delta K210/\Delta K210}$ hearts. Each data point represents an individual animal (n=4). * denotes $p<0.05$ (Mann-Whitney test) comparing CCR2- to CCR2+ macrophages. **H-I**, Immunostaining for CD68 (green), FAK (white), and troponin (red) reveals evidence of focal adhesion complexes at sites of macrophage-cardiomyocyte interaction. Each data point represents an individual animal (n=12 per experimental group). * denotes $p<0.05$ (Mann-Whitney test) compared to controls.

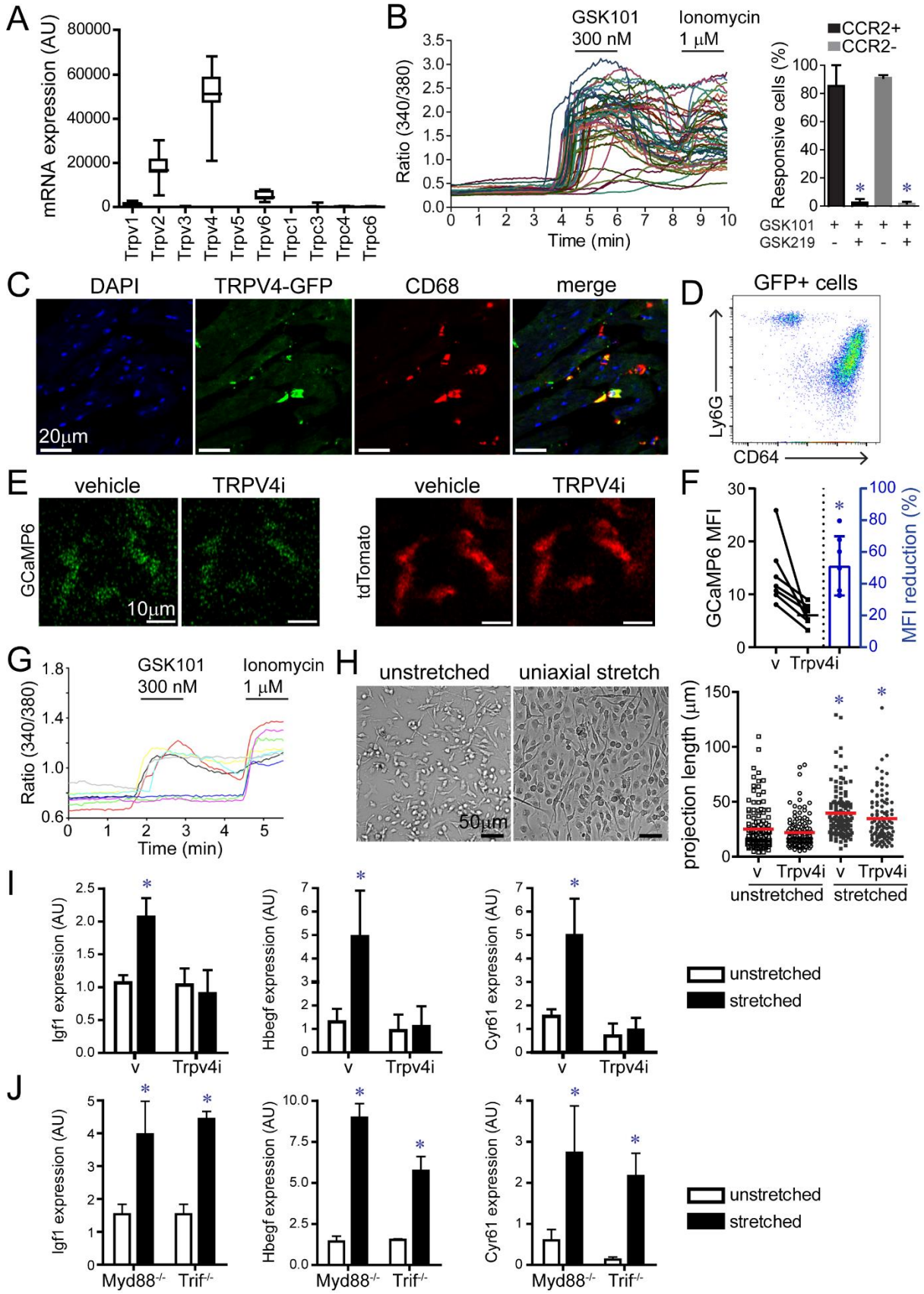

Figure 7. The mechanoresponsive TRPV4 channel regulates growth factor expression in macrophages. A, mRNA expression of TRP channels in CCR2- macrophages showing robust expression of Trpv4. Data generated from n=20 samples. **B**, Ratiometric calcium assay demonstrating that cardiac macrophages have active TRVP4 channels. GSK101: TRPV4 agonist, GSK219: TRPV4 antagonist. * denotes $p<0.05$ comparing GSK101 treated cells with GSK101 and GSK219 treated cells. **C**, Immunostaining of TRPV4-GFP BAC transgenic mice showing GFP (green) expression in CD68+ macrophages (red) within the LV myocardium. **D**, Flow cytometry of cardiac CD45+GFP+ leukocytes isolated from TRPV4-GFP heart revealing that macrophages and neutrophils express TRPV4. Repetitive images from n=4 mice. **E**, 2-photon imaging of GFP (green) and tdTomato (red) in papillary muscle preparations harvested from CX3CR1-ertCre; Rosa26-GCaMP6/tdTomato mice treated with either vehicle or the TRPV4 inhibitor GSK219 (TRPV4i). **F**, Quantification of GCaMP6 signal. Each data point represent mean data from an individual experiment (n=6). * denotes $p<0.05$ compared to vehicle. **G**, Ratiometric calcium assay showing that bone marrow derived macrophages express active TRPV4 channels. GSK101: TRPV4 agonist, Ionomycin: calcium ionophore. **H**, Cyclic uniaxial stretch (1 Hz, 10% deformation, 24 hours) promotes elongation of bone marrow derived macrophages independent of TRPV4 channel activity. n=4 independent experiments. **I**, Quantitative RT-PCR assays demonstrating that cyclic uniaxial stretch promotes increased Igf1, Hbegf, and Cyr61 mRNA expression in bone marrow-derived macrophages. Upregulation of Igf1, Hbegf, and Cyr61 mRNA expression by uniaxial cyclic stretch is dependent on TRPV4 channel activity. n=4 independent experiments. **J**, Quantitative RT-PCR assays demonstrating that Igf1, Hbegf, and Cyr61 mRNA expression by uniaxial cyclic stretch is independent of MYD88 and TRIF signaling pathways. n=4 independent experiments. * denotes $p<0.05$ compared to vehicle treated unstretched cells (ANOVA post-hoc Tukey) (F-H). Error bars denote standard deviation (G-H).

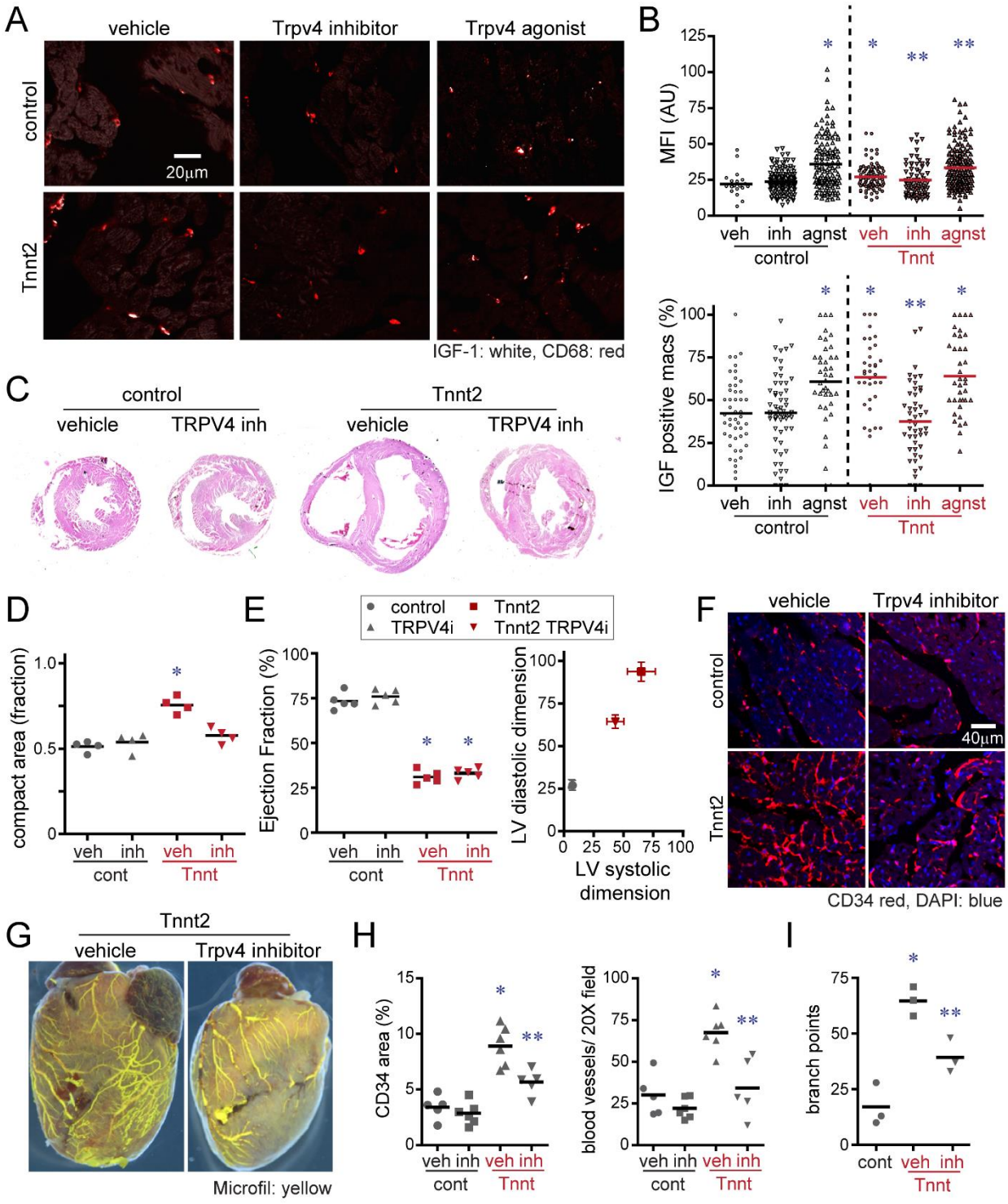

Figure 8. TRPV4 channel activity regulates IGF1 expression in CCR2- macrophages and is required for coronary angiogenesis. A, Immunostaining for IGF1 (white) and CD68 (red) in the LV myocardium of control and Tnnt2$^{\Delta K210/\Delta K210}$ mice treated with either vehicle, TRPV4 inhibitor, or TRPV4 agonist demonstrating that TRPV4 channel activity regulates macrophage IGF1 protein expression *in vivo*. **B**, Quantification of IGF1 protein expression (% IGF1+ macrophages, IGF1 MFI) in control and Tnnt2$^{\Delta K210/\Delta K210}$ hearts treated with either vehicle, TRPV4 inhibitor, or TRPV4 agonist. MFI: mean florescent intensity. Each data point represents an analyzed 20X field. n=5 animals per experimental group (A-B). * denotes $p<0.05$ compared to vehicle treated control hearts. ** denotes $p<0.05$ compared to vehicle treated Tnnt2$^{\Delta K210/\Delta K210}$ hearts. (ANOVA, post-hoc Tukey). **C**, Low magnification H&E images of control and Tnnt2$^{\Delta K210/\Delta K210}$ mice treated with either vehicle or TRPV4 inhibitor for 2 weeks beginning at 6 weeks of age. LV in cross-section (n=4 per experimental group). **D**, Quantification of the ratio of compact to trabecular myocardium in control and Tnnt2$^{\Delta K210/\Delta K210}$ mice treated with either vehicle or TRPV4 inhibitor. Each data point represents an individual animal. * denotes $p<0.05$ compared to vehicle treated control hearts (ANOVA, post-hoc Tukey). **E**, Echocardiographic assessment of LV ejection fraction and LV chamber dimensions in control and Tnnt2$^{\Delta K210/\Delta K210}$ mice treated with either vehicle or TRPV4 inhibitor for 2 weeks beginning at 6 weeks of age. n=5 per experimental group. * denotes $p<0.05$ compared to vehicle treated control hearts (ANOVA, post-hoc Tukey). **F**, Immunostaining for CD34 (red) in the LV myocardium of control and Tnnt2$^{\Delta K210/\Delta K210}$ mice treated with either vehicle or TRPV4 inhibitor showing that TRPV4 channel activity contributes to coronary microvascular expansion in Tnnt2$^{\Delta K210/\Delta K210}$ hearts. **G**, Microfil vascular casting showing that TRPV4 channel activity is necessary for expansion of coronary microvasculature in Tnnt2$^{\Delta K210/\Delta K210}$ hearts. **H-I**, Quantification of coronary microvasculature (G) and coronary microvasculature (H) in the designated experimental groups. Each data point represents an individual animal (n=5 per experimental group). * denotes $p<0.05$ compared to vehicle treated control. ** denotes $p<0.05$ compared to all other groups (ANOVA, post-hoc Tukey).